

NASA CR-165, 79.3



NASA Contractor Report 165793

NASA-CR-165793

1982 0004268

BIAXIAL TESTS OF FLAT GRAPHITE/EPOXY
LAMINATES

Harold Liebowitz and Douglas L. Jones

THE GEORGE WASHINGTON UNIVERSITY
School of Engineering and Applied Science
Washington, DC 20052

Grant NSG-1289
October 1981

LIBRARY COPY

NOV 18 1981

LANGLEY RESEARCH CENTER
LIBRARY, NASA
HAMPTON, VIRGINIA



National Aeronautics and
Space Administration

Langley Research Center
Hampton, Virginia 23665

SUMMARY

This report summarizes the research performed under NASA Grant NSG1289 Improved Fracture Toughness Determination for Aircraft Structural Materials, over the life of the Grant, February 1, 1976, to December 31, 1980. The Technical Officers of this Grant were Drs. Wolf Elber and G. L. Roderick of the NASA Langley Research Center.

The primary purpose of this research program was to examine analytically and experimentally the influence of biaxially applied loads on the strength of composite materials containing holes. The analysis was performed through the development of a three-dimensional, finite-element computer program that is capable of considering three types of damage: fiber breakage, delamination, and matrix failure. Realistic failure criteria were established for each of the failure modes and the influence of biaxial loading on damage accumulation under monotonically increasing loading was examined in detail.

The experimental portion of this program encompassed both static and fatigue testing of specially designed biaxial specimens containing central holes. Initially, static tests were performed to obtain an understanding of the influence of biaxial loads on the fracture strength of composite materials and to provide correlation with the analytical predictions. The predicted distributions and types of damage were in reasonable agreement with the experimental results. Then a number of fatigue tests were performed to determine the influence of cyclic biaxial loads on the fatigue life and residual strength of several composite laminates.

N82-12141 #

LIST OF SYMBOLS

ϕ_i = the angle between X-axis and the fiber orientation in the i-th layer

σ_{ij} = stress tensor

ϵ_{ij} = strain tensor

S_{ijmn} = material constants for linear elastic anisotropic solid

(L,T,z) = coordinate system; L-axis is parallel to the fiber orientation; z-axis is perpendicular to the laminate

E_L, E_T = Young's moduli

ν_{LT}, ν_{Tz} = Poisson's ratios

G_{LT}, G_{Tz} = shear moduli

d_{ij} = material constants for elastic solid with axis symmetry expressed in (L,T,z) coordinate system

d'_{ij} = material constants for elastic solid with axis symmetry expressed in (x,y,z) coordinate system

u_x, u_y, u_z = displacements in x,y,z direction, respectively

t_i = stress vector

n_i = unit normal vector of a surface

(r,θ,z) = cylindrical coordinate system

r_0 = radius of the centered hole

$[\delta]$ = nodal point displacement vector

N_1, N_2, \dots, N_8 = shape functions

ξ, η, ζ = nondimensional coordinates for a three dimensional prism

$[B]$ = matrix linking strains and nodal point displacement vector

$[J]$ = Jacobian matrix

$[F]$ = nodal point force vector

$[K]$ = stiffness matrix

$\sigma_L, \sigma_T, \sigma_z, \sigma_{LT}, \sigma_{Lz}, \sigma_{Tz}$ = stress components in (L,T,z) coordinate system

$\sigma_{FN}, \sigma_{FS}, \sigma_{MN}, \sigma_{MS}, \sigma_{DN}, \sigma_{DS}$ = failure strengths of a unidirectional fiber-reinforced composite layer

R_1, R_2, \dots, R_6 = ratios between stresses and failure strengths

$R[I]$ = damage ratio of the I-th element

R_{\max} = maximum damage ratio of the entire laminate

σ = applied stress

k = biaxial load factor

$2L, 2W, 2h$ = Total length, width, height of the laminate

INTRODUCTION

The research program, Improved Fracture Toughness Determination for Aircraft Structural Materials, was initiated for the purpose of studying several problems of interest to NASA. The grant, NSG1289, was sponsored through the NASA Langley Research Center (LaRC) over the period February 1, 1976, to December 31, 1980.

The initial task of this grant was to perform a detailed assessment of several nonlinear fracture toughness parameters, with the emphasis to be placed on the two-parameter Newman method. This assessment was completed and the results reported to LaRC in September, 1976.

The second and most important task was to evaluate both analytically and experimentally the effect of biaxial applied loads on composite laminates containing holes. In order to perform this research it was necessary to develop a comprehensive three-dimensional, finite-element program and an experimental facility capable of applying substantial biaxial loads on composite specimens. Both of these capabilities were established and subsequently employed in this research program. The primary emphasis of this program was placed on multilayer composite materials in which the individual plies were oriented at $0, \pm 45$ and 90 degrees from an axis of symmetry. This configuration is approximately isotropic in its material behavior

and because of this property has been widely employed in aerospace structures. In addition, some testing has been performed on $[0, \pm 45, 0]_{ns}$ laminates ($n = 1, 2$).

Both the analytical and experimental tasks emphasized specimens containing central holes, since they provide free surfaces at which the damage is expected to initiate. The diameter of the central hole was not varied in the analysis, although the hole diameter-to-specimen width ratio ($2r_0/2w$) could easily be varied in subsequent computations. Since the test specimen size was fixed, some experiments were performed with different hole diameters so that the influence of hole size could also be examined.

The emphasis in the finite-element analysis was placed on monotonically increasing loading, because of the difficulty and expense of applying three-dimensional, finite-element programs to fatigue problems. Therefore, the initial experiments were also performed statically for the purpose of obtaining comparisons with the experimental results. In addition, a substantial number of fatigue tests were performed, so that an understanding could be obtained of biaxial load effects on the fatigue life and residual strength of composite specimens with holes. The principal results of the analytical and experimental results are discussed in greater detail in subsequent sections of this report.

FINITE-ELEMENT ANALYSIS OF LAYERED COMPOSITE MATERIALS

One of the two primary objectives of this grant was the development of a three-dimensional, finite-element computer program to analyze damage accumulation in composite laminates. This program has been developed and is capable of:

- (i) providing a detailed stress distribution in a structural member made of a layered fiber-reinforced composite material containing a round hole and subjected to biaxial applied loading;
- (ii) identifying the shape and extent of the damage zone and the mode of failure; and
- (iii) analyzing the problem of accumulated damage and progressive failure for any given failure criterion.

The principal characteristics of this program are outlined in the subsections below.

Problem Description

The specimen geometry is that of a rectangular plate made from a layered composite material containing a centered circular hole and subjected to in-plane biaxial loading. Each layer is a unidirectional fiber reinforced composite material oriented at some angle ϕ with respect to an axis of symmetry (the x-axis). The input data for a graphite-epoxy laminate are given below.

1. Material Constants

$$E_L = 134.58 \times 10^3 \text{ MPa}$$

$$E_T = 9.68 \times 10^3 \text{ MPa}$$

$$\nu_{LT} = 0.264$$

$$\nu_{TZ} = 0.435$$

$$G_{LT} = 4.48 \times 10^3 \text{ MPa}$$

2. Ply Configuration

$$[0,45,-45,90]_s$$

3. Specimen Parameters

$$2L = 152.4 \text{ mm}$$

$$2W = 152.4 \text{ mm}$$

$$2h = 1.07 \text{ mm}$$

$$r_0 = 12.7 \text{ mm}$$

4. Finite-Element Mesh

$$\text{Number of nodal points} = 1750$$

$$\text{Number of degrees of freedom} = 5250$$

$$\text{Number of elements} = 1248$$

The coordinate directions are defined in Fig. 1.

Linear Elastic Theory

Each layer is modeled as a linear elastic continuum having an axis of symmetry about its fiber orientation.

Until delamination occurs the layers are assumed to be perfectly bonded together. No adhesive layer is included in this study.

Finite-Element Method

The finite-element mesh consists of a family of three-dimensional prisms, each having eight nodes. Each node is assumed to have three degrees of freedom of motion. The symmetry and periodicity of this geometry have been taken into consideration. The initial results of this analysis have been published by Lee [1].

Failure Criteria

It was assumed that only three types of damage can occur in this laminate: fiber breakage, debonding, and matrix failure. Failure criteria (strengths) associated with each mode of failure are given below

$$\sigma_{FN} = 1241 \text{ MPa}$$

$$\sigma_{FS} = 82.7 \text{ MPa}$$

$$\sigma_{MN} = 55.2 \text{ MPa}$$

$$\sigma_{MS} = 82.7 \text{ MPa}$$

$$\sigma_{DN} = 55.2 \text{ MPa}$$

$$\sigma_{DS} = 89.6 \text{ MPa}$$

The stress components are defined in Fig. 1.

The Numerical Procedure

An iterative procedure has been devised to identify the damaged zone and the mode of failure. After this has been done, the appropriate constraining forces are reduced to zero and the local stiffness matrix of the damaged zone is modified according to the mode of failure. Then the stress distribution is recalculated to determine whether the damage is progressing. When the damage is determined to be propagating the ultimate strength of the laminate is then assumed to be known as a function of the specific biaxial load ratio.

The detailed formulation, analysis, and the numerical results are contained in a paper entitled, "Three Dimensional Finite-Element Analysis of Damage Accumulation in Composite Laminate," which has been accepted for publication in Computers and Structures [2]. A copy of this paper is included as Appendix A of this report. The principal conclusions of this paper are listed below.

- (1) The initial stress distribution of σ_T near the edge of the hole determines the location of the initial damage zone and its mode of failure as well as the applied stress necessary to cause initial damage.
- (2) The initial stress distribution of σ_L near the edge of the hole predicts the final path of fracture.
- (3) No delamination was identified at any time in the failure process.

EXPERIMENTAL PROGRAM

The primary objective of the experimental portion of this research program has been to establish a data base which would serve to identify the effects of biaxially applied loads on the failure characteristics of composite materials. The experimental research program required the following initial steps to get the test system into operation:

- (i) the design and fabrication of a biaxial testing system,
- (ii) the design of a suitable test specimen or specimens, and
- (iii) the performance of some initial tests on metal specimens to check out the test system.

These tasks were completed early in the research program as indicated in the early progress reports. The test system developed for these tests is illustrated in Fig. 2 and the general specimen geometry is shown in Fig. 3. A more detailed description of the system development was provided in an earlier progress report [3]. In addition, the results of a number of tests on metals and polymers have been reported [4].

After the test system was determined to be functioning properly, five test series were conducted in the following sequence.

- (1) Four initial static strength tests were performed on graphite/epoxy specimens, having $[0, \pm 45, 90]_s$ and $[0, \pm 45, 90]_{2s}$ configurations, in which central hole diameters of 12.70 and 50.80 mm were utilized. The primary purpose of these tests was to determine whether variations in hole size influenced either the strength or the magnitude of the biaxial effect, for $k = 0$ and 1.0 .
- (2) Seven additional static strength tests were performed on graphite/epoxy specimens having $[0, \pm 45, 90]_s$, $[0, \pm 45, 90]_{2s}$ and $[0, \pm 45, 0]_{2s}$ configurations as a further evaluation of biaxial and hole size effects. Center hole diameters of 25.4 and 50.8 mm and biaxialities of $k = 0, 1/2$, and 1.0 were used in these tests.
- (3) After evaluation of the breaking strengths of the first eleven specimens, a series of seven fatigue tests were conducted on $[0, \pm 45, 0]_s$, and $[0, \pm 45, 0]_{2s}$ laminates. The test conditions for these specimens were: center hole diameters - 25.4 and 50.8 mm; loading frequency - 10Hz in-phase cyclic loading; and biaxiality ratio - $k = 0, 0.25$ and 0.50 .

- (4) A series of one static and five fatigue tests was performed on six additional specimens having a $[0, \pm 45, 90]_s$ configuration. The static test was performed for the purpose of comparing with earlier specimens having the same layup pattern. The test parameters for the fatigue tests were similar to the previous fatigue tests except that the biaxiality ratios were $k = 0, 0.5, \text{ and } 1.0$.
- (5) A series of one static and five fatigue tests was performed on six specimens having the $[0, \pm 45, 0]_s$ layup pattern. The initial static test in this series was different from the previous ones in that the loading rate was the same as that for the cyclic tests (10Hz) whereas the previous static tests had been performed slowly (for data-taking purposes). The remaining fatigue tests were performed as in the earlier tests for this layup except that 50.8 mm diameter center holes were used for all specimens.

After all of the test results had been evaluated, their variations with biaxiality ratio, hole diameter, thickness, etc., were collected and examined. These results are included in this report, along with the conclusions drawn from them.

Test System Development

The biaxial test system illustrated in Fig. 2 was developed by fabricating a special, light-weight test frame of 222,400 N (50,000 lb.) capacity and interfacing it with an existing 444,800 N (100,000 lb.) capacity test system used as the vertical axis. Both systems were of the servo-hydraulic type so that both static and dynamic loads could be applied to either axis. An additional control system was added that has the capability of controlling both axis and special equipment was added to eliminate interaction or "cross-talk" between the two channels. Since only two hydraulic actuators were used in this system, the center of the test specimen would not remain stationary but would move in response to each actuator. In order to prevent this motion from introducing side loads onto the specimen the horizontal axis was suspended in its working position by elastic ropes. The deformation and pendulum action permitted by the ropes permitted slight movement in both the vertical and horizontal directions with the center of the specimen. Although the motion of the frame under rapid cycling transmits dynamic inertial loads to the specimen, the magnitudes of these loads were calculated for expected worst-case conditions and were found to be small enough to be neglected.

A biaxial test specimen was designed as a modification of an existing specimen configuration used elsewhere [5-7]. A

photoelastic study was initiated for the purpose of maximizing the size of the central uniformly-stressed work area. It was also necessary to design and purchase (or fabricate) grips to interface between the test system and the specimen. The specially designed grips that were purchased performed satisfactorily throughout the testing program.

After assembly of the horizontal test system, it was operated for a brief check-out period and then interconnected with the existing vertical test system. The combined system was then checked out and found to operate as designed. This system design permitted phased operation of the two channels as well as completely independent operation.

Experimental Procedure

While the test system was being developed, the characteristics (material, layup, etc.) of the various test specimens were determined through discussions between the technical officer and one of the principal investigators. A typical specimen is shown in Fig. 4, where it is seen that a reinforcing aluminum sheet was bonded to each side of the specimen in the area around the four loading tabs. The specimens were manufactured by a separate vendor to the specifications agreed upon by the technical officer and principal investigator.

While the specimens were being prepared, the test con-

ditions (hole diameter, biaxiality ratio, loading conditions, etc.) were also established for the first test series of four static tests. A total of thirty specimens, all made of 5208-T300 graphite/epoxy lamina, were prepared and tested under this program. The characteristics and test conditions for these specimens are shown in Table 1. Biaxiality ratios were limited to the range $0 \leq k \leq 1.0$ for two reasons: (i) the quasi-isotropic $[0, \pm 45, 90]_{ns}$ configuration is symmetric with respect to the horizontal and vertical axes, so that the reciprocal biaxiality ratios, $\infty < k \leq 1.0$ are also included in these tests, and (ii) the $[0, \pm 45, 0]_{ns}$ configuration was limited to ratios of $0 \leq k \leq 0.5$, because of its reduced strength in the 90° orientation.

The specimen design shown in Fig. 4 created one type of difficulty that had considerable influence on some of the test parameters. The problem was caused by the tendency of some specimens to fail by tearing off one or more of the loading tabs, resulting in the lack of failure through the test section. These tests could not provide valid results so certain modifications were introduced into the specimen design to reduce the tendency for tab failures. The problem was particularly bothersome in the $[0, \pm 45, 0]_{ns}$ specimens because the tabs in the 90° orientation would fail under quite small biaxiality ratios. Because of this problem most of the later tests employed hole diameters of 50.8 mm. This modification was still inadequate for several tests so

additional modifications were introduced. The most successful modification was to machine away the reinforcing aluminum beyond where the individual tabs were separated. A specimen modified by these procedures is shown in Fig. 5 and such modifications were employed in many of the later tests. The problem of tab tear-off was also greater for the fatigue tests than for the static tests.

Test procedures unique to each test series are now discussed in some detail so that the significance of the results may be more fully appreciated.

Test Series (1)

This test series was comprised of four static strength tests on the quasi-isotropic laminates involving variations in thickness (8 and 16 ply laminates), hole diameter, ($D = 12.7$ and 50.8 mm) and biaxiality ratio, $k = 0$ and 1.0 . The loads were applied as in-phase ramp functions having 300 second duration. The ramp functions were interrupted periodically to record data manually from digital multimeters. Five channels of data were recorded, including load and stroke on each axis and the hole opening displacement in the primary (largest load) direction. Load displacement curves in the primary direction were also recorded using an x-y recorder. All specimens failed through the center hole.

Test Series (2)

Upon satisfactory completion of the first four tests, seven additional static tests were performed on both the quasi-isotropic and the $[0, \pm 45, 0]_{2s}$ configurations. The first two tests were performed to examine the influence of fabrication damage, which existed in a number of the specimens, around the central hole. The most extensively damaged specimen was 9-2 and the extent of the damage is indicated in Fig. 6a. Identical test conditions were applied to specimens 9-2 and 9-3 (which had negligible damage around the hole), with the test results indicating that the initial damage did not influence the strength. The breaking strength was slightly greater for 9-2 and the final fracture occurred away from the initial damage, as seen in Fig. 6b. As a result of these tests, the existing initial damage was not taken into consideration in the subsequent testing.

Specimens 5-3, 5-4 and 5-5 represented a test series in which only the biaxial load ratio was varied. The material was quasi-isotropic and biaxial ratios of 0, 0.5 and 1.0 were selected. The tests were performed using in-phase ramp functions on each axis and all failures traversed through the center holes.

Specimens 11-1 and 11-2 also represented a biaxial static strength series for the $[0, \pm 45, 0]_{2s}$ configuration. Biaxial ratios of $k = 0$ and 0.5 were employed for these tests and the failures traversed through the center holes.

Test Series (3)

This test series was comprised of seven fatigue tests on the $[0, \pm 45, 0]_{2s}$ and $[0, \pm 45, 0]_s$ configurations. The purpose of these tests was to determine whether damage accumulation due to cyclic loading at low biaxiality ratios would have any significant influence on the strength in the 0° fiber orientation. Based on the static strength tests already performed on the $[0, \pm 45, 0]_{2s}$ configuration (Specimens 11-1 and 11-2), the first specimen (11-3) in this series was fatigue cycled in uniaxial tension at 75 percent of the ultimate strength obtained from Specimen 11-1. The specimen had not failed after 10^6 cycles so the residual strength was measured following the same procedures as for the static strength tests. The next specimen was fatigue cycled under the same load in the 0° direction but with $k = 0.5$ rather than 0. This specimen failed quickly by tearing off one of the horizontal tabs (90° direction) and thus did not represent a strictly valid biaxial comparison. The third specimen was cycled at the same primary load level as before but with $k = 0.25$. This specimen failed after approximately 440,000 cycles by pulling off one of the primary-axis tabs so it also could not represent a valid biaxial comparison.

Because of the difficulties encountered in obtaining valid biaxial comparisons in the three previous tests, the next four tests (Specimens 7-1, 7-3, 7-4, and 7-5 in the

$[0, \pm 45, 0]_s$ configuration) were employed primarily for determining a modified specimen design capable of eliminating the tab failure problem. All four tests were performed with a biaxiality ratio of 0.25. The first specimen was tested without modification as a check on the necessity of specimen modification for the eight-ply configuration. The applied cyclic loading for 7-1 was selected to be 80 percent of the strength of the corresponding sixteen-ply specimens and the biaxiality ratio was $k = 0.25$. This specimen sustained 10^6 cycles after which the residual strength was evaluated and found to be significantly greater than the estimated original strength. This specimen failed through the center hole and along one edge so it was considered to represent a valid failure. The next specimen (7-3) was modified by increasing the center hole diameter from 25.4 to 50.8 mm and was tested at a considerably higher cyclic load. It failed after approximately 3×10^5 cycles by tearing off two adjacent loading tabs and so did not provide valid comparisons. The next specimen (7-4) was modified by increasing the depth of the twenty slots between the individual loading tabs to the edge of the aluminum reinforcing plate. The slots were extended for two purposes: (i) to further reduced the net section of the specimen through the center hole, and (ii) to prevent the initial cracking of the aluminum from contributing to stress concentration effects. This specimen failed

during cyclic loading by tearing off two adjacent loading tabs. Some of the damage extended to the center hole but the failure did not pass through it.

The final specimen in this series was also modified by increasing the central hole diameter to 50.8 mm and extending the slot depth as was done for the previous test. This specimen also failed by pulling off two perpendicular tangs, although the 0° direction tab failure extended through the center hole. This test was thus considered to be marginally successful in performing the desired objective. A photograph of the fractured specimen is shown in Fig. 7.

Test Series (4)

This test series was comprised of one static and five fatigue tests on specimens having the quasi-isotropic $[0, \pm 45, 90]_s$ configuration. The first test was a static test for the purpose of comparing the strength with prior tests of the same configuration. The test conditions for this specimen, 23-1, were identical to specimen 5-3 and the ultimate loads were in very good agreement with each other. Since there was no evidence that the quasi-isotropic specimens had a tendency for failure at the tabs, a fatigue test was performed at 80 percent of the ultimate ($k = 0$ in both cases) and the specimen failed at approximately 218,000 cycles by tearing off one of the tabs in the primary

direction. It is possible that the failure was due to a momentary overload caused by a power failure in the laboratory so the absolute value of the cyclic life was not reliable. Since the failure did not occur through the center hole, the test would not have been suitable for comparison purposes. For the remaining four specimens the center hole diameter was increased to 50.8 mm to increase the probability of center failures. The next three tests (23-3, 23-4, 23-6) represent the influence of biaxial loads ($k = 0, 0.5$ and 1.0) on the fatigue life and all three provided valid data. The final test, 23-5, was listed at a value of $k = 0.5$ and sustained 10^6 cycles. The residual strength was tested and found to be quite high. However, this specimen failed by breaking off of two perpendicular tabs and the corner of the test area between them. Since the fracture did not go through the center hole the results were not considered to be valid.

Test Series (5)

This test series was comprised of one static strength test and five fatigue tests on specimens having the $[0, \pm 45, 0]_s$ configuration. By the time that this test series was conducted, a PDP-11-03 computer had been added to the system for the purpose of rapid data collection. Therefore, it was decided that the static test would be performed at a rate of 10Hz, rather than at the low rates previously

employed. It was hoped that a test of this type would provide a more accurate measure of the ultimate strength and thus improve the accuracy of the percent of ultimate stress used in performing the fatigue tests. Also, because of the prior problems encountered with tab failure, two modifications of these specimens were made: (i) the hole diameter was increased from 25.4 to 50.8 mm, and (ii) the aluminum reinforcing plate was machined away to approximately 6.3 mm beyond the slot tips without disturbing the composite material. These modifications were successful, since all six specimens failed through the center hole. A photograph of one of the modified specimens is shown in Fig. 5. Specimens 24-2 and 24-3 were loaded at 80 percent and 90 percent, respectively, of the ultimate strength determined from specimen 24-1. Both of these specimens sustained 10^6 cycles and provided high residual strengths. The biaxial ratio was 0.25 for all three tests.

The final three tests represented a series of three fatigue life tests in which the biaxial ratio had the values, $k = 0, 0.1, \text{ and } 0.25$. All three specimens were loaded at least 90 percent of the static strength obtained from specimen 24-1 and all failed in less than 10^3 cycles. Thus, the results were not as conclusive as they would have been if there had been a greater spread of fatigue lives. Nevertheless the tests appeared to be valid and do provide a measure of the influence of biaxial ratio on the fatigue life.

Results

The results of the various types of tests and specimen parameter variations have been collected together in tabular form as shown in Tables 2-5. These tables illustrate the results of similar tests on each laminate and how the mechanical property examined was influenced by various material and test parameters. The parameters examined were hole diameter, biaxial load factor, thickness, and type of specimen modification. The mechanical properties examined were the static or ultimate strength, the fatigue life, and the residual strength. The details of each property variation will be discussed on the basis of its variation illustrated in the accompanying tables.

Static Strength Variations

Although it was not a primary part of this study, an initial series of static tests was performed in which the hole diameter was varied from 12.7 to 50.8 mm to determine the significance of any hole diameter influence on the static strength. These tests were performed on the quasi-isotropic configurations in both the eight and sixteen ply thicknesses. Thus these tests were expected to provide indications of both hole diameter and specimen thickness influences on the static strength of these materials.

All static and residual strength calculations, as well

as the applied stress level determinations, are based on the applied force divided by the net section area A_{NET} . The net section width is taken to be the distance between the tips of the stress equalization slots minus the diameter of the center hole. The stress concentration factors associated with the holes were ignored since they were the same for all tests and would thus not affect any of the comparisons. An example of the stress calculations is included here so that there will be no misunderstanding of the implications of the subsequent comparisons.

Specimen 5-1.

Uniaxial tension: $k = 0$

Hole diameter: 12.75 mm

Net section area:

$$(A_{NET}): 171.20 - 12.75 = 158.45 \times 1.11 = \underline{175.88 \text{ mm}^2}$$

Failure load (F_c): 64,500 N

$$\text{Critical stress: } \sigma_c = \frac{F_c}{A_{NET}} = \frac{64,500}{175.88} = \underline{367 \text{ MPa}} .$$

The influence of hole diameter variation on the static strength of $[0, \pm 45, 90]_s$ laminates is shown in Table 2. The biaxial load ratio, k , was equal to zero for all of these tests. It is seen that the static strength decreases slightly as D increases from 12.7 to 25.4 mm and then increases as D is increased to 50.8 mm. However, the entire variation is less than 20 percent so the effect does not

appear to be of extreme importance. It is also noted that the two identical tests 5-3 and 23-1, which were conducted from different specimen lots and over a time interval of many months, provided results that were nearly identical.

A similar series of tests was performed on the 16 ply quasi-isotropic laminate, $[0, \pm 45, 90]_{2s}$ and the results are seen in Table 3. The biaxial load ratio, k was equal to 1.0 for all of these tests. The same pattern seen in Table 2 also exists in Table 3. The static strength decreased slightly and then increased, although the breaking strengths for $D = 12.7$ and $D = 50.8$ mm were approximately equal in this case. If the values for the identical tests 9-2 and 9-3 are averaged, the maximum variation is less than ten percent. The average strength values from Tables 2 and 3 are 375 and 454 MPa, respectively. While this represents a significant difference, it cannot be attributed to any single effect because both the thickness and the biaxiality are different. It is suspected that most of the difference is due to the biaxial effect but there is not adequate data to verify this conclusion.

Since the principal thrust of this research program was the determination of biaxial load effects, two test series provided data about the biaxial effect as seen in Table 4. These tests exhibit a significant influence of applied load biaxiality, for the $[0, \pm 45, 90]_s$ laminates, while the results are negligible for the $[0, \pm 45, 0]_{2s}$ tests. For the eight ply quasi-isotropic laminates, Table 4 shows that the residual

strength increases approximately 50 percent as k increases from 0 to 1.0. These results coincided with a change in fracture path from perpendicular to the primary load axis to approximately 45° to it. However, it is not suggested that the resolved area be used to reduce the magnitude of the biaxial effect because it has not yet been possible to examine this matter in adequate detail.

A pair of tests which provided an indication of the biaxial effect for the $[0, \pm 45, 0]_{2s}$ laminates are also included in Table 4. The k variation was limited to the range 0 to 0.5 because of the weakness of this laminate in the 90° orientation. It is evident that no biaxial effect exists in these two tests, but additional tests are needed to confirm or disprove this behavior.

Fatigue Tests

A number of fatigue tests have been performed to ascertain the possible extent of cyclic load biaxiality on the fatigue life and residual strength. For these tests the specimens were subjected to in-phase cyclic loads at a frequency of 10Hz until they failed, or until 10^6 cycles were sustained. Any specimens lasting for 10^6 cycles were then tested for their residual strength. The results of both the fatigue life and residual strength tests are seen in Table 5. In general the objective was to apply cyclic loads at levels of 70-80 percent of the static ultimate strength. However,

the results given in Table 5 indicate that an extremely broad range of cyclic lives were found to exist.

The results of the test series on the $[0, \pm 45, 0]_{2s}$ laminates indicate a very strong and detrimental influence of load biaxiality on the fatigue life. However, as noted in the table, Specimens 11-5 and 11-4 did not fail through the center hole but failed due to the breaking of the loading tabs. Thus it seems evident that the biaxial effect would not have been nearly as great if the premature tab failures had not occurred. Because of this difficulty with tab failures, the series of four specimens, 7-1, 7-3, 7-4 and 7-5, was devoted to specimen modifications intended to enhance specimen failures through the center hole. These attempts were only marginally successful so they are not discussed in this section.

The results of a series of fatigue tests on $[0, \pm 45, 90]_s$ laminates, in which only the biaxial load ratio is varied, are also presented in Table 5. These tests showed that both the uniaxial and equal biaxial tests resulted in relatively short fatigue lives. However, the test with $k = 0.5$ resulted in a cyclic life approximately ten times the $k = 0$ and $k = 1.0$ results. Because of this behavior an additional test, 23-5, was performed with $k = 0.5$, which displayed even greater resistance to fatigue failure. The appearance of the broken specimens suggested that these results may represent a valid biaxial effect. The $k = 0$ and $k = 1.0$ specimens both failed

in a rather brittle fashion along planes parallel to one of the layers (the 90° and 45° directions). However, the specimens with $k = 0.5$ failed at an angle between the 90° and 45° directions only after a very extensive amount of damage had been accumulated. It was thus concluded that when the preferred failure plane coincided with a ply orientation the failure could occur with relative ease. However, when failure along another plane would be anticipated a considerable amount of damage accumulation is necessary, thus resulting in a longer fatigue life. These tentative conclusions are also in need of further verification.

The results of the last series of fatigue tests on $[0, \pm 45, 0]_s$ laminates are also shown in Table 5. As discussed previously, all of these specimens had been modified as shown in Fig. 5. This modification was successful in eliminating the problem of tab failure, but the results were still not without inconsistency.

It is seen from Table 5 that the general trend of these fatigue lives was toward increasing fatigue lives with increasing biaxiality in the range $0 \leq k \leq 0.25$. However, the differences between tests 24-2 and 24-3 on one hand and 24-4, 24-5 and 24-6 are immense, being more than three orders of magnitude in the fatigue life without taking into consideration the considerable residual strength. It is possible that the residual strength of test 24-3 was improperly recorded, since it was obtained only from a peak-reading

digital indicator which has sometimes given erratic readings in the past. The conclusion which may be validly drawn from these tests is that the fatigue life does, in fact, increase with increasing biaxiality in the range tested. The fractured specimens displayed the same trend as the 23 series, in which the amount of damage accumulated by the specimens was much greater when the failure could not occur along one of the fiber directions. Thus, it is expected that the fatigue life would begin to decrease as the biaxial factors increased beyond 0.25.

CONCLUSIONS

A combined theoretical and experimental research program has been performed to examine the influence of biaxial applied loads on the mechanical properties of composite materials.

The theoretical program consisted of developing a multi-layer finite-element program for examining the stress and damage distributions in composite laminates subjected to biaxial applied loads. The program was developed and operated with the following results.

- (1) The initial stress distribution normal to the fiber direction, but in the plane of the layer, near the hole determines the location of the initial damage zone and the applied stress necessary to cause failure.
- (2) The initial stress distribution in the fiber direction near the hole predicts the failure path.
- (3) No delamination was predicted although it does occur early in the actual failure process.

Five series of biaxial fracture toughness tests, comprised of 30 specimens, have been performed with the following conclusions.

- (1) The size of the center hole did not have a strong influence on the failure load.

- (2) Applied load biaxiality had a significant influence on the static strength of $[0, \pm 45, 90]_{ns}$ laminates but a negligible influence on the $[0, \pm 45, 0]_{ns}$ laminates.
- (3) Biaxial cyclic loads had a very significant influence on the cyclic life, although in some cases the influence was positive while others it was inconsistent or negative. The difference in behavior was determined by the manner in which the biaxial load altered the direction of the fracture path.

LIST OF REFERENCES

- [1] J. D. Lee, Three Dimensional Finite Element Analysis of Layered Fiber-Reinforced Composite Materials, Computers and Structures, 12, pp. 319-339 (1980).
- [2] J. D. Lee, Three Dimensional Finite Element Analysis of Damage Accumulation in Composite Laminate. To appear in Computers and Structures.
- [3] H. Liebowitz and D. L. Jones, Semi-Annual Progress Report, March 1 - August 31, 1978, NASA Langley Research Center Grant NSG 1289.
- [4] D. L. Jones and J. Eftis, Final Scientific Report, October 1, 1976 - May 30, 1980, Air Force Office of Scientific Research Grant AFOSR 76-3099.
- [5] J. C. Radon, P. S. Leever and L. E. Culver, A Simple Testing Technique for Fracture Under Biaxial Stress, Experimental Mechanics, 17, pp. 228-232, 1977.
- [6] C. D. Hopper and K. J. Miller, Fatigue Crack Propagation in Biaxial Stress Fields, J. Strain Analysis, 12, pp. 23-28, 1977.
- [7] I. M. Daniel, Behavior of Graphite/Epoxy Plates With Holes Under Biaxial Loading, Experimental Mechanics, 20, pp. 1-8, 1980.

TABLE 1. Characteristics and Test Conditions of
5208-T300 Graphite/Epoxy Biaxial Specimens

TEST SERIES	SPECIMEN NUMBER	LAMINA ORIENTATIONS	BIAXIALITY RATIO k	HOLE DIAMETER D(mm)	TYPE OF TEST*
1	5-1	$[0, \pm 45, 90]_s$	0	12.75	1
	5-2	"	"	50.98	"
	9-4	$[0, \pm 45, 90]_{2s}$	1.0	"	"
	9-5	"	"	12.75	"
2	9-2	$[0, \pm 45, 90]_{2s}$	1.0	25.53	1
	9-3	"	"	"	"
	5-3	$[0, \pm 45, 90]_s$	0	"	"
	5-4	"	0.50	"	"
	5-5	"	1.0	"	"
	11-1	$[0, \pm 45, 0]_{2s}$	0	25.55	"
3	11-2	"	0.50	"	"
	11-3	$[0, \pm 45, 0]_{2s}$	0	25.48	3
	11-4	"	0.50	25.53	2
	11-5	"	0.25	"	"
	7-1	$[0, \pm 45, 0]_s$	"	25.55	3
	7-3	"	"	50.80	2
	7-4	"	"	25.53	"
	7-5	"	"	50.93	"
4	23-1	$[0, \pm 45, 90]_s$	0	25.47	1
	23-2	"	"	25.45	2
	23-3	"	"	50.80	"
	23-4	"	0.50	"	"
	23-5	"	"	"	3
	23-6	"	1.0	"	2
5	24-1	$[0, \pm 45, 0]_s$	0.25	50.80	4
	24-2	"	"	"	3
	24-3	"	"	"	"
	24-4	"	"	"	2
	24-5	"	0.10	"	"
	24-6	"	0	"	"

* 1 - Static strength test at low load rate.

2 - Fatigue life test.

3 - Residual strength test after 10^6 fatigue cycles.

4 - Static strength test at high load rate.

TABLE 2. Effect of Center Hole Diameter on the Static Strength of $[0, \pm 45, 90]_s$ Laminates

SPECIMEN NUMBER	BIAXIALITY RATIO	HOLE DIAMETER (mm)	BREAKING LOAD (N X 10^3)	STATIC STRENGTH (MPa)
5-1	0	12.75	64.5	366
5-3	"	25.53	55.2	349
23-1	"	25.45	56.9	356
5-2	"	50.98	55.6	429

TABLE 3. Effect of Center Hole Diameter on the Static Strength of $[0, \pm 45, 90]_{2s}$ Laminates

SPECIMEN NUMBER	BIAXIALITY RATIO	HOLE DIAMETER (mm)	BREAKING LOAD (N X 10^3)	STATIC STRENGTH (MPa)
9-5	1.0	12.75	161	473
9-2	"	25.53	133	405
9-3	"	25.53	144	439
9-4	"	50.98	128	472

TABLE 4. Effect of Applied Load Biaxiality on the Static Strength of $[0, \pm 45, 90]_s$ and $[0, \pm 45, 90]_{2s}$ Laminates

SPECIMEN NUMBER	BIAXIALITY RATIO	HOLE DIAMETER (mm)	BREAKING LOAD (N X 10^3)	STATIC STRENGTH (MPa)
$[0, \pm 45, 90]_s$ Laminates				
5-3	0	25.53	55.2	349
23-1	"	25.45	56.9	356
5-4	0.5	25.53	64.9	405
5-5	1.0	"	81.0	507
$[0, \pm 45, 0]_{2s}$ Laminates				
11-1	0	25.55	161	505
11-2	0.5	"	162	505

TABLE 5. Effect of Cyclic Load Biaxiality on the Fatigue Life and Residual Strength of Composite Laminates

SPECIMEN NUMBER	BIAXIALITY RATIO	CYCLIC STRESS LEVEL (MPa)	FATIGUE LIFE (Cycles X 10 ³)	RESIDUAL STRENGTH (MPa)
[0,±45,0] _{2s} Laminates				
11-3	0	377	1000	514
11-5*	0.25	370	442	---
11-4*	0.50	378	23	---
[0,±45,90] _s Laminates				
23-3	0	338	29	---
23-4	0.5	339	447	---
23-5*	"	341	1000	416
23-6	1.0	343	42	---
[0,±45,0] _s Laminates				
24-6	0	335	0.15	---
24-5	0.10	338	0.50	---
24-4	0.25	356	0.44	---
24-3	"	332	1000	451
24-2	"	305	1000	392

* Specimen did not fail through center hole.

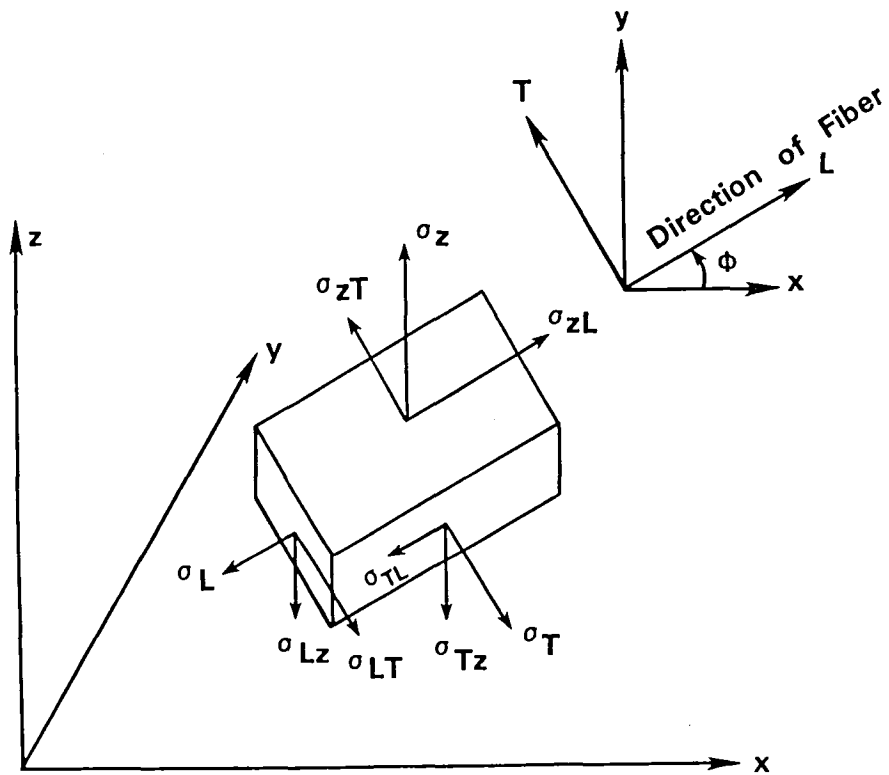


Fig. 1. Stress components on the L, T, z coordinate system.

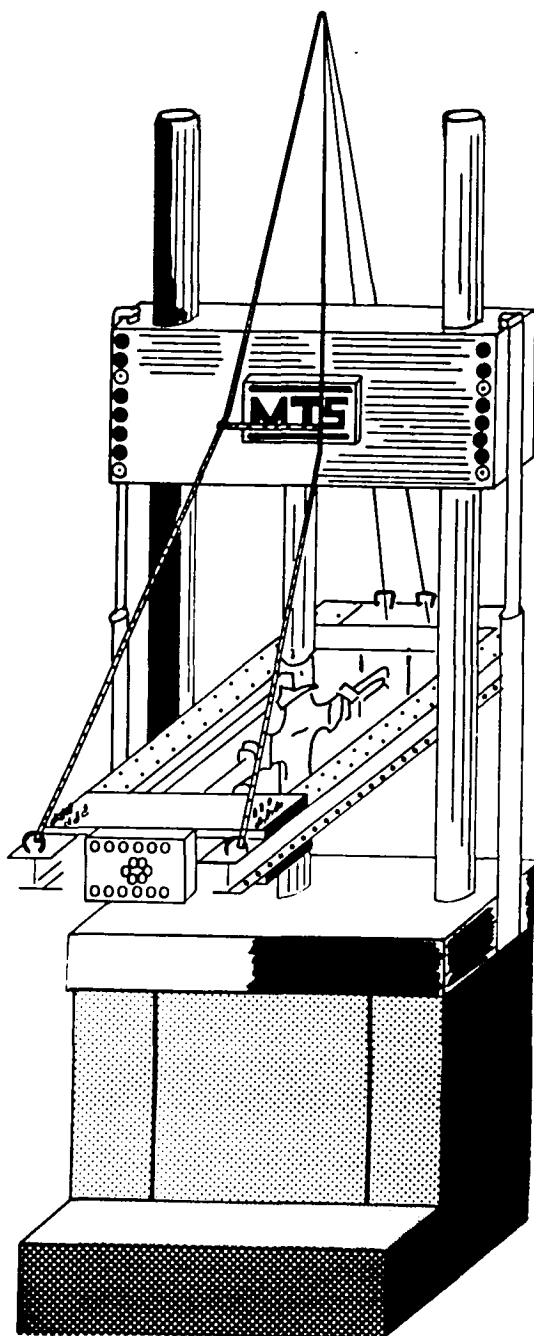


Figure 2. Biaxial test system.

Figure 3. Biaxial specimen design.

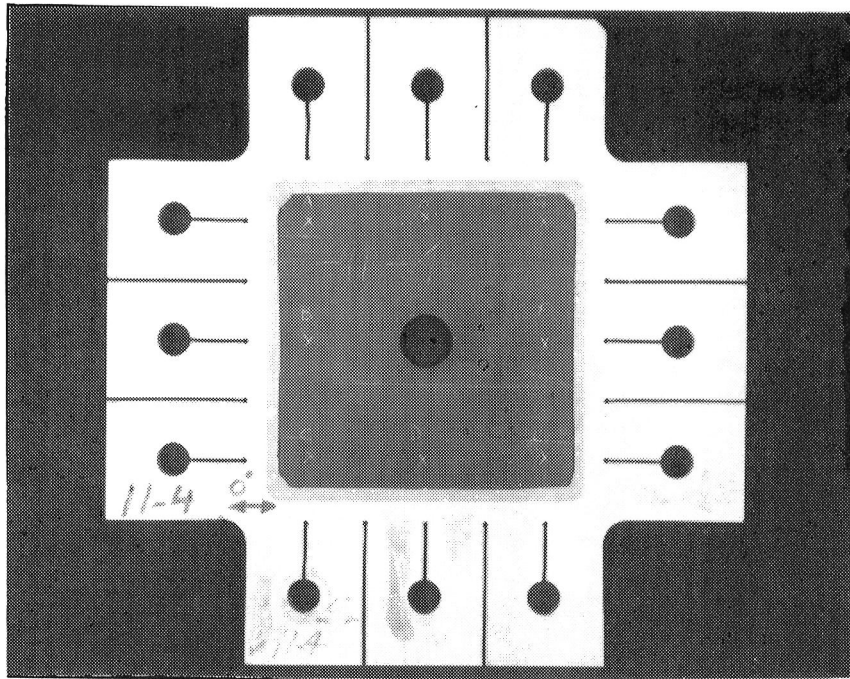


Fig. 4. Photograph of typical specimen prior to testing.

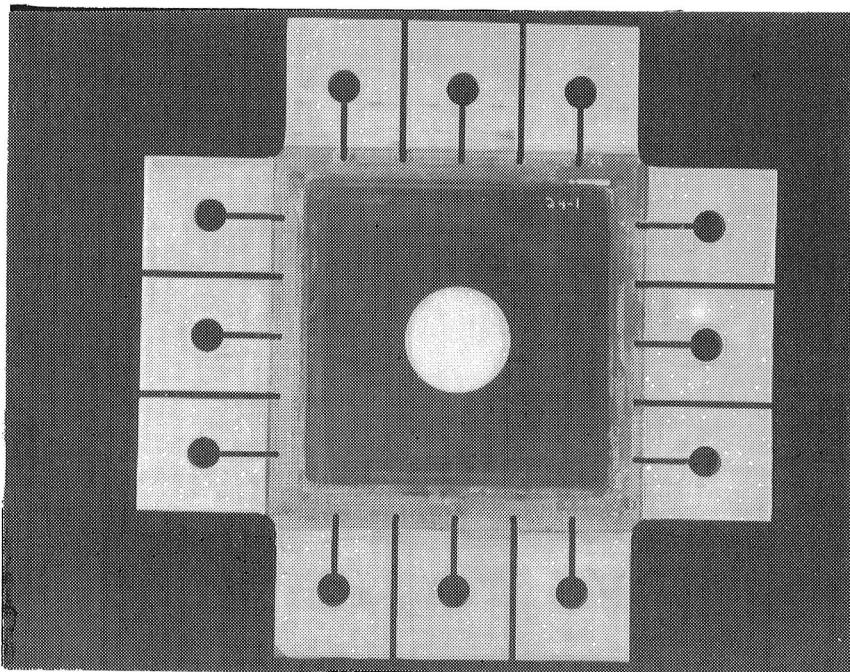
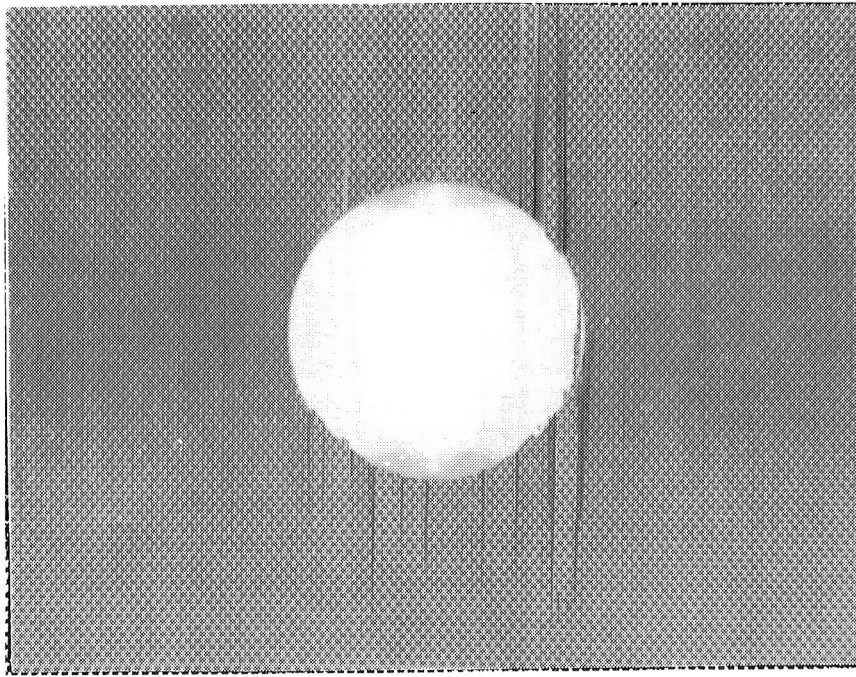
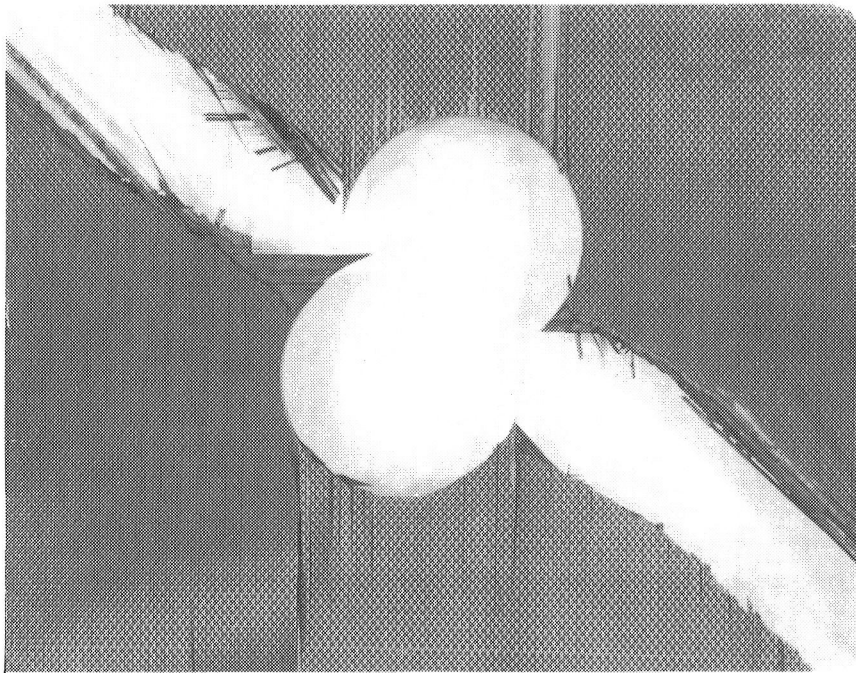


Fig. 5. Modification of specimen to reduce tab failures.



(a)



(b)

Fig. 6. Close-up photograph of specimen 9-2 showing, (a) prior damage and (b) final fracture condition.

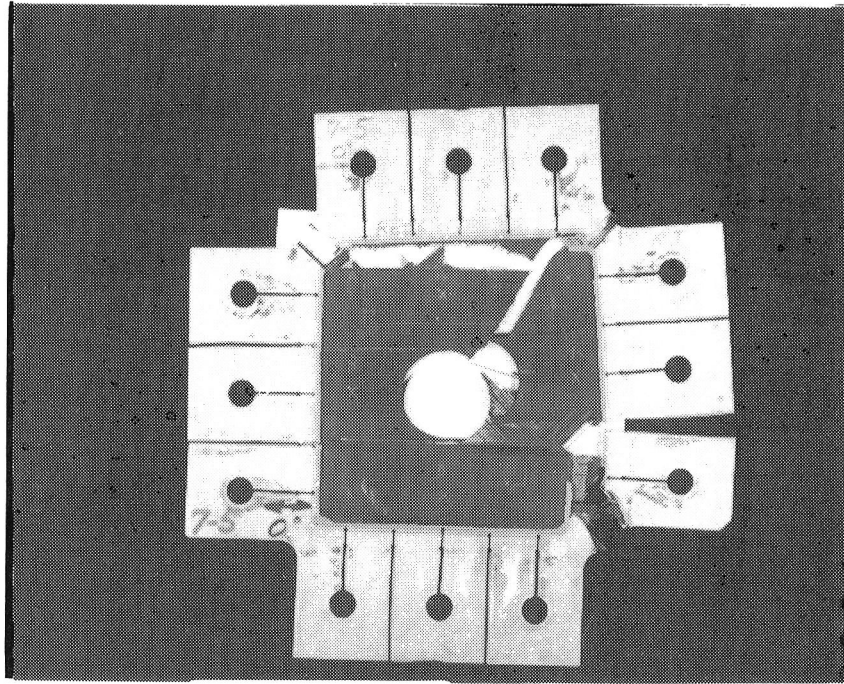


Fig. 7. Photograph of fractured specimen 7-5 showing other modifications.

A P P E N D I X

4
5
6
7
8

9
10
11
12

THREE DIMENSIONAL FINITE ELEMENT
ANALYSIS OF DAMAGE ACCUMULATION
IN COMPOSITE LAMINATE

James D. Lee

School of Engineering and Applied Science
The George Washington University
Washington, D.C. 20052

10

10

ABSTRACT

A three dimensional finite-element computer program has been developed to analyze layered fiber-reinforced composite laminate. This program is capable of: (1) calculating the detailed stress distribution, (2) identifying the damage zone and mode of failure, (3) analyzing the damage accumulation, and (4) determining the ultimate strength of the composite laminate.

4
5
6
7
8

9
10
11
12
13

1. INTRODUCTION

The high strength and light weight properties of composite materials are causing them to assume increasing structural applications in all weight-sensitive structures, especially aircraft and aerospace structures. These same properties are also leading to increased utilization in other areas of the transportation sector, such as automobiles, where the reduction of weight leads to greater gasoline economy. Thus, as the structural applications of composite materials increase, the necessity of knowing more about their mechanical properties, especially their failure characteristics becomes more urgent.

In the past two decades, together with the creations of new composite materials and the developments of new fabrication techniques, various aspects of physical properties of composite materials have been investigated and different approaches for the better understanding of the material behaviors have been proposed. These efforts are published in the Journal of Composite Materials, ASTM proceedings, textbooks, and other periodicals. It is worthwhile to mention the work of Wendt et al. [1], Calcote [2], Garg et al. [3], Chamis [4], and Jones [5].

Since composite materials are heterogeneous and anisotropic, the analysis of small-scale specimens or

full-size structural elements made of composites is much more difficult than that of homogeneous and isotropic materials. Only in the most recent years, the development of techniques in numerical analysis together with large capacity and high speed computers make it possible to analyze layered fiber-reinforced composite laminates in detail [6-9].

Lee performed a three-dimensional stress analysis for a biaxially loaded composite laminate (with a centered hole), which consists of several fiber-reinforced composite layers each with a specified fiber orientation, by finite element method [10]. In this work, a more sophisticated computer program was developed to analyze the damage accumulation including progressive failure of a layered fiber-reinforced composite laminate and to determine the ultimate strength of the composite laminate. This computer program is written in STAR-FORTRAN language and was operated on the CDC STAR-100 computer system at the NASA-Langley Research Center, Hampton, Virginia.

2. PROBLEM DESCRIPTION

Let the specimen under consideration be a rectangular plate made of layered composite material, with a centered circular hole, subjected to in-plane biaxial loading (Fig. 1). Each layer is a unidirectional fiber reinforced composite and the direction of the fiber is characterized by the angle ϕ between the fiber and x-axis. Thus, the arrangement of n layers for the entire laminate can be represented by $[\phi_1, \phi_2, \dots, \phi_n]$. In this paper, attention is focused on a symmetric ply configuration which may be denoted as:

$$[\phi_1, \phi_2, \dots, \phi_i]_s \equiv [\phi_i, \dots, \phi_2, \phi_1, \phi_1, \phi_2, \dots, \phi_i] \quad (2.1)$$

The top four plies of a symmetric ply configuration $[0, 45, -45, 90]_s$ is shown in Fig. 2.

It is noted that the symmetric configuration has a mirror symmetry with respect to the x-y plane at $z=0$ and a periodicity of 180° about z-axis [10]. If the loading condition also has the same characteristics, only a quarter of the entire laminate needs to be analyzed.

Two basic assumptions are made in this analysis:

1. Each layer is modeled as a linear elastic continuum with transverse anisotropy about fiber orientation; individual fibers and matrix are not considered;
2. Unless delamination occurs, the layers are assumed to be perfectly bonded together; no adhesive layer is included in this study.

3. STRESS-STRAIN RELATION

The general stress-strain relation for a linear elastic anisotropic solid can be written as [11]:

$$\epsilon_{ij} = S_{ijmn} \sigma_{mn} , \quad (3.1)$$

where

$$S_{ijmn} = S_{jimn} = S_{ijnm} = S_{mnij} . \quad (3.2)$$

The number of independent elastic constants is 21. Material symmetry, when it exists, imposes restrictions on the material constants, thus further reducing the number of independent elastic constants. Since, for each layer, the unidirectional fiber reinforced composite has a axis of symmetry about the fiber orientation, the number of independent elastic constants is reduced to five and, in engineering notation, the stress-strain relation could be expressed as:

$$\begin{vmatrix} \epsilon_L \\ \epsilon_T \\ \epsilon_z \\ \gamma_{Tz} \\ \gamma_{zL} \\ \gamma_{LT} \end{vmatrix} = \begin{vmatrix} E_L^{-1} & -\nu_{LT}E_L^{-1} & -\nu_{LT}E_L^{-1} & 0 & 0 & 0 \\ -\nu_{LT}E_L^{-1} & E_T^{-1} & -\nu_{Tz}E_T^{-1} & 0 & 0 & 0 \\ -\nu_{LT}E_L^{-1} & -\nu_{Tz}E_T^{-1} & E_T^{-1} & 0 & 0 & 0 \\ 0 & 0 & 0 & G_{Tz}^{-1} & 0 & 0 \\ 0 & 0 & 0 & 0 & G_{LT}^{-1} & 0 \\ 0 & 0 & 0 & 0 & 0 & G_{LT}^{-1} \end{vmatrix} \begin{vmatrix} \sigma_L \\ \sigma_T \\ \sigma_z \\ \sigma_{Tz} \\ \sigma_{zL} \\ \sigma_{LT} \end{vmatrix}, \quad (3.3)$$

where $G_{Tz} = 0.5 E_T / (1 + \nu_{Tz})$ and L-axis denotes the fiber orientation. The (L,T,z) coordinate system is shown in Fig. 3. Now it is straightforward to obtain

$$\begin{vmatrix} \sigma_L \\ \sigma_T \\ \sigma_z \\ \sigma_{Tz} \\ \sigma_{zL} \\ \sigma_{LT} \end{vmatrix} = \begin{vmatrix} d_{11} & d_{12} & d_{13} & 0 & 0 & 0 \\ d_{12} & d_{22} & d_{23} & 0 & 0 & 0 \\ d_{13} & d_{23} & d_{33} & 0 & 0 & 0 \\ 0 & 0 & 0 & d_{44} & 0 & 0 \\ 0 & 0 & 0 & 0 & d_{55} & 0 \\ 0 & 0 & 0 & 0 & 0 & d_{66} \end{vmatrix} \begin{vmatrix} \epsilon_L \\ \epsilon_T \\ \epsilon_z \\ \gamma_{Tz} \\ \gamma_{zL} \\ \gamma_{LT} \end{vmatrix}, \quad (3.4)$$

where

$$\begin{aligned}
d_{11} &= E_L(1 - \nu_{TZ}^2)/\Delta , \\
d_{22} &= d_{33} = E_T(1 - \nu_{LT}^2 E_T/E_L)/\Delta , \\
d_{12} &= d_{13} = E_T(1 + \nu_{TZ}) \nu_{LT}/\Delta , \\
d_{23} &= E_T(\nu_{TZ} + \nu_{LT}^2 E_T/E_L)/\Delta , \\
d_{44} &= G_{TZ} , \\
d_{55} &= d_{66} = G_{LT} , \\
\Delta &= 1 - \nu_{TZ}^2 - 2\nu_{LT}^2(1 + \nu_{TZ}) E_T/E_L .
\end{aligned} \tag{3.5}$$

For a composite layer, whose fiber orientation is denoted by ϕ , the general stress-strain relation is obtained as [10]:

$$\begin{vmatrix} \sigma_x \\ \sigma_y \\ \sigma_z \\ \sigma_{yz} \\ \sigma_{zx} \\ \sigma_{xy} \end{vmatrix} = \begin{vmatrix} d'_{11} & d'_{12} & d'_{13} & 0 & 0 & d'_{16} \\ d'_{12} & d'_{22} & d'_{23} & 0 & 0 & d'_{26} \\ d'_{13} & d'_{23} & d'_{33} & 0 & 0 & d'_{36} \\ 0 & 0 & 0 & d'_{44} & d'_{45} & 0 \\ 0 & 0 & 0 & d'_{45} & d'_{55} & 0 \\ d'_{16} & d'_{26} & d'_{36} & 0 & 0 & d'_{66} \end{vmatrix} \begin{vmatrix} \epsilon_x \\ \epsilon_y \\ \epsilon_z \\ \gamma_{yz} \\ \gamma_{zx} \\ \gamma_{xy} \end{vmatrix} , \tag{3.6}$$

where

$$d'_{11} = d_{11}\cos^4\phi + d_{22}\sin^4\phi + 2(d_{12} + 2d_{66})\sin^2\phi\cos^2\phi ,$$

$$d'_{22} = d_{11}\sin^4\phi + d_{22}\cos^4\phi + 2(d_{12} + 2d_{66})\sin^2\phi\cos^2\phi ,$$

$$d'_{33} = d_{33} ,$$

$$d'_{44} = d_{44}\cos^2\phi + d_{55}\sin^2\phi ,$$

$$d'_{55} = d_{44}\sin^2\phi + d_{55}\cos^2\phi ,$$

$$d'_{66} = d_{66} + (d_{11} + d_{22} - 2d_{12} - 4d_{66})\sin^2\phi\cos^2\phi ,$$

$$d'_{12} = d_{12} + (d_{11} + d_{22} - 2d_{12} - 4d_{66})\sin^2\phi\cos^2\phi , \quad (3.7)$$

$$d'_{13} = d_{13}\cos^2\phi + d_{23}\sin^2\phi ,$$

$$d'_{23} = d_{13}\sin^2\phi + d_{23}\cos^2\phi ,$$

$$d'_{16} = \sin\phi\cos\phi[d_{11}\cos^2\phi - d_{22}\sin^2\phi - \cos 2\phi(d_{12} + 2d_{66})] ,$$

$$d'_{26} = \sin\phi\cos\phi[d_{11}\sin^2\phi - d_{22}\cos^2\phi + \cos 2\phi(d_{12} + 2d_{66})] ,$$

$$d'_{36} = \sin\phi\cos\phi(d_{13} - d_{23}) ,$$

$$d'_{45} = \sin\phi\cos\phi(d_{55} - d_{44}) .$$

4. BOUNDARY CONDITIONS

In this work, attention is focused on a special kind of loading condition which is indicated in Fig. 1. That special kind of loading condition does have a mirror symmetry with respect to x-y plane at $z = 0$ and a periodicity of 180° about z-axis. Thus, it is obvious to have the following relations

$$\begin{aligned} u_x(-x, -y, z) &= -u_x(x, y, z) , \\ u_y(-x, -y, z) &= -u_y(x, y, z) , \\ u_z(-x, -y, z) &= u_z(x, y, z) . \end{aligned} \tag{4.1}$$

Based on eqns. (4.1) and (3.6), it is straightforward to derive [10]:

$$\begin{aligned} \sigma_x(-x, -y, z) &= \sigma_x(x, y, z) , \\ \sigma_y(-x, -y, z) &= \sigma_y(x, y, z) , \\ \sigma_z(-x, -y, z) &= \sigma_z(x, y, z) , \\ \sigma_{xy}(-x, -y, z) &= \sigma_{xy}(x, y, z) , \\ \sigma_{zx}(-x, -y, z) &= -\sigma_{zx}(x, y, z) , \\ \sigma_{zy}(-x, -y, z) &= -\sigma_{zy}(x, y, z) . \end{aligned} \tag{4.2}$$

Therefore, it is only needed to analyze a quarter of the entire laminate, which is shown in Fig. 4.

Referring to Fig. 4, for any point, pt. $I(x,y,z)$, on the surface S_I , there is a conjugate point, pt. $J(-x,-y,z)$, on the surface S_J ; both surfaces S_I and S_J have the same unit normal vector $(n_x, n_y, 0)$. The stress vector, \underline{t} , at a point on either S_I or S_J is related to the stress tensor at that point and the unit normal vector of that surface as follows:

$$t_i = \sigma_{ij}n_j , \quad (4.3)$$

or, specifically,

$$\begin{aligned} t_x &= \sigma_x n_x + \sigma_{xy} n_y , \\ t_y &= \sigma_y n_y + \sigma_{xy} n_x , \\ t_z &= \sigma_{zx} n_x + \sigma_{zy} n_y . \end{aligned} \quad (4.4)$$

Then the boundary conditions on surfaces S_I and S_J may be specified as:

$$\begin{aligned} u_x(I) &= -u_x(J) , \quad t_x(I) = t_x(J) , \\ u_y(I) &= -u_y(J) , \quad t_y(I) = t_y(J) , \\ u_z(I) &= u_z(J) , \quad t_z(I) = -t_z(J) . \end{aligned} \quad (4.5)$$

The rest of the boundary conditions simply are:

1. On top surface, $z = h$,

$$\sigma_z = \sigma_{zx} = \sigma_{zy} = 0 ; \quad (4.6)$$

2. On symmetric surface, $z = 0$,

$$u_z = \sigma_{zx} = \sigma_{zy} = 0 ; \quad (4.7)$$

3. On surfaces S_1 , and S_2 , $x = \pm W$,

$$\sigma_x = k\sigma , \sigma_{xz} = \sigma_{xy} = 0 ; \quad (4.8)$$

4. On surface S_3 , $y = L$,

$$\sigma_y = \sigma , \sigma_{yx} = \sigma_{yz} = 0 ; \quad (4.9)$$

5. On surface of the centered hole, $r = r_0$,

$$\sigma_{rr} = \sigma_{r\theta} = \sigma_{rz} = 0 ; \quad (4.10)$$

where σ and k will be called the applied stress and the biaxial load factor. The stress boundary conditions specified in eqns. (4.5-4.10) were converted into equivalent nodal force boundary conditions for use in the computer program.

5. FINITE ELEMENT ANALYSIS

In this work, the three dimensional finite element mesh consists of a family of 8-node elements. A typical element with the nodal points being numbered for the purpose of discussion is shown in Fig. 5. Let $[\delta] \equiv [u_1, u_2, \dots, u_8]^T$ be the nodal point displacement vector and

$$[u_i] \equiv \begin{bmatrix} u_x(i) \\ u_y(i) \\ u_z(i) \end{bmatrix}, \quad i = 1, 2, \dots, 8. \quad (5.1)$$

The shape functions are

$$\begin{aligned} N_1 &= (1 + \xi)(1 - \eta)(1 + \zeta)/8, \\ N_2 &= (1 + \xi)(1 + \eta)(1 + \zeta)/8, \\ N_3 &= (1 - \xi)(1 - \eta)(1 + \zeta)/8, \\ N_4 &= (1 - \xi)(1 + \eta)(1 + \zeta)/8, \\ N_5 &= (1 + \xi)(1 - \eta)(1 - \zeta)/8, \\ N_6 &= (1 + \xi)(1 + \eta)(1 - \zeta)/8, \\ N_7 &= (1 - \xi)(1 - \eta)(1 - \zeta)/8, \\ N_8 &= (1 - \xi)(1 + \eta)(1 - \zeta)/8. \end{aligned} \quad (5.2)$$

Then the displacement field within this element can be written as:

$$[u_x, u_y, u_z]^T = [\phi_1, \phi_2, \dots, \phi_8][\delta] , \quad (5.3)$$

where

$$[\phi_i] = \begin{vmatrix} N_i & 0 & 0 \\ 0 & N_i & 0 \\ 0 & 0 & N_i \end{vmatrix} , \quad i = 1, 2, \dots, 8 . \quad (5.4)$$

The strain field $[\epsilon] \equiv [\epsilon_x, \epsilon_y, \epsilon_z, \gamma_{yz}, \gamma_{zx}, \gamma_{xy}]^T$ is then related to the nodal point displacement vector as

$$[\epsilon] = [B_1, B_2, \dots, B_8][\delta] \equiv [B][\delta] , \quad (5.5)$$

where, for $i = 1, 2, \dots, 8$,

$$[B_i] = \begin{vmatrix} N_{i,x} & 0 & 0 \\ 0 & N_{i,y} & 0 \\ 0 & 0 & a_i/\Delta z \\ 0 & a_i/\Delta z & N_{i,y} \\ a_i/\Delta z & 0 & N_{i,x} \\ N_{i,y} & N_{i,x} & 0 \end{vmatrix} , \quad (5.6)$$

$$a_i \equiv \partial N_i / \partial z . \quad (5.7)$$

And the coordinates (x,y) and (ξ,η) are linked by

$$\begin{bmatrix} N_{i,\xi} \\ N_{i,\eta} \end{bmatrix} = \begin{bmatrix} \partial x / \partial \xi & \partial y / \partial \xi \\ \partial x / \partial \eta & \partial y / \partial \eta \end{bmatrix} \begin{bmatrix} N_{i,x} \\ N_{i,y} \end{bmatrix} = [J] \begin{bmatrix} N_{i,x} \\ N_{i,y} \end{bmatrix}, \quad (5.8)$$

where, referring to Fig. 5,

$$[J] = \frac{1}{4} \begin{bmatrix} (1-\eta)(x_1-x_3) + (1+\eta)(x_2-x_4) & (1-\eta)(y_1-y_3) + (1+\eta)(y_2-y_4) \\ (1+\xi)(x_2-x_1) + (1-\xi)(x_4-x_3) & (1+\xi)(y_2-y_1) + (1-\xi)(y_4-y_3) \end{bmatrix}.$$

Then the element equation which links the nodal point displacement vector $[\delta]$ and the nodal point force vector $[F]$ can be written as [12]:

$$[K] [\delta] = [F], \quad (5.9)$$

where

$$\begin{aligned} [K] &= \int_V [B]^T [d'] [B] dV, \\ &= \int_{-1}^1 \int_{-1}^1 \int_{-1}^1 [B]^T [d'] [B] \Delta z \det[J] d\xi d\eta d\zeta, \end{aligned} \quad (5.10)$$

and $[d']$ is specified in eqn. (3.6). The final governing equation is simply the sum of all the element equations.

6. THE FAILURE CRITERION

After the governing equation of the laminate has been solved, the components of displacement for each nodal point can be obtained and then the six components of stress $[\sigma] \equiv [\sigma_x, \sigma_y, \sigma_z, \sigma_{yz}, \sigma_{zx}, \sigma_{xy}]^T$ at any point within a certain element can be found as

$$[\sigma] = [d'] [B] [\delta] . \quad (6.1)$$

The stress components in (L,T,z) coordinate system can be written as

$$\sigma_L = \sigma_x \cos^2 \phi + \sigma_y \sin^2 \phi + \sigma_{xy} \sin 2\phi , \quad (6.2)$$

$$\sigma_T = \sigma_x \sin^2 \phi + \sigma_y \cos^2 \phi - \sigma_{xy} \sin 2\phi , \quad (6.3)$$

$$\sigma_z = \sigma_z , \quad (6.4)$$

$$\sigma_{LT} = (\sigma_y - \sigma_x) \sin \phi \cos \phi + \sigma_{xy} \cos 2\phi , \quad (6.5)$$

$$\sigma_{Lz} = \sigma_{xz} \cos \phi + \sigma_{yz} \sin \phi , \quad (6.6)$$

$$\sigma_{Tz} = -\sigma_{xz} \sin \phi + \sigma_{yz} \cos \phi . \quad (6.7)$$

To identify the damage zone, attention is focused on three types of damage: breakage of fibers, failure of matrix, and separation of layers (delamination). The failure criterion for these three modes is discussed as follows:

1. Fiber Breakage

For this failure mode, the stresses at the center of each element are taken as the representative of that element. An element is identified as the damage zone of broken fibers if either

$$\sigma_L \geq \sigma_{FN} , \quad (6.8)$$

or

$$\sigma_{LS} \equiv (\sigma_{LT}^2 + \sigma_{LZ}^2)^{\frac{1}{2}} \geq \sigma_{FS} . \quad (6.9)$$

In either case, the stiffness matrix of that element, referring to eqn. (3.4), will be reduced to zero.

2. Matrix Failure

For this failure mode, the stresses at the center of each element are taken as the representative of that element. An element is identified as the damage zone of matrix failure if either

$$\sigma_T \geq \sigma_{MN} , \quad (6.10)$$

or

$$\sigma_{TS} \equiv (\sigma_{TL}^2 + \sigma_{TZ}^2)^{\frac{1}{2}} \geq \sigma_{MS} \quad (6.11)$$

In either case, some components in the stiffness matrix of that element are reduced to zero, i.e.,

$$[d] = \begin{bmatrix} d_{11} & 0 & d_{13} & 0 & 0 & 0 \\ 0 & 0 & 0 & 0 & 0 & 0 \\ d_{13} & 0 & d_{33} & 0 & 0 & 0 \\ 0 & 0 & 0 & 0 & 0 & 0 \\ 0 & 0 & 0 & 0 & d_{55} & 0 \\ 0 & 0 & 0 & 0 & 0 & 0 \end{bmatrix}, \quad (6.12)$$

which means σ_T , σ_{Tz} , and σ_{LT} of that element will be reduced to zero irrespective of the strain field.

3. Delamination

For this failure mode, the stresses at the center of the interface between two layers are taken as the representative for the interface of the two adjacent elements. An interface of those two adjacent elements is identified as the damage zone of delamination if either

$$\sigma_z \geq \sigma_{DN}, \quad (6.13)$$

or

$$\sigma_{zS} \equiv (\sigma_{Lz}^2 + \sigma_{Tz}^2)^{\frac{1}{2}} \geq \sigma_{DS}. \quad (6.14)$$

In either case, some components in the stiffness matrix of those two elements are reduced to zero, i.e.,

$$[d] = \begin{bmatrix} d_{11} & d_{12} & 0 & 0 & 0 & 0 \\ d_{12} & d_{22} & 0 & 0 & 0 & 0 \\ 0 & 0 & 0 & 0 & 0 & 0 \\ 0 & 0 & 0 & 0 & 0 & 0 \\ 0 & 0 & 0 & 0 & 0 & 0 \\ 0 & 0 & 0 & 0 & 0 & d_{66} \end{bmatrix}, \quad (6.15)$$

which means σ_z , σ_{Tz} , and σ_{zL} of those two elements will be reduced to zero irrespective of the strain field.

The failure strength, σ_{FN} , σ_{FS} , σ_{MN} , σ_{MS} , σ_{DN} , and σ_{DS} , should be obtained experimentally and taken as the input data for the computer program. Checking the stresses at the center of each element and the stresses at the center of interface of each element permits the identification of the damage zone and its mode of failure for a specified amount of applied stress.

7. THE PROCEDURES

To begin with, fix the biaxial load factor k and set the applied stress σ to be unit. After the governing equation of the laminate has been solved, it is straightforward to find the representative stresses for each element and for each interface of two elements of adjacent layers, $\sigma_L, \sigma_{LS}, \sigma_T, \sigma_{TS}, \sigma_z, \sigma_{zS}$. Define six ratios R_1, R_2, \dots, R_6 as follows:

$$\begin{aligned}
 R_1 &\equiv \sigma_L / \sigma_{FN} , \\
 R_2 &\equiv \sigma_{LS} / \sigma_{FS} , \\
 R_3 &\equiv \sigma_T / \sigma_{MN} , \\
 R_4 &\equiv \sigma_{TS} / \sigma_{MS} , \\
 R_5 &\equiv \sigma_z / \sigma_{DN} , \\
 R_6 &\equiv \sigma_{zS} / \sigma_{DS} .
 \end{aligned} \tag{7.1}$$

Then, for each element and its associated interface, the damage ratio, $R(I)$, is defined as

$$R(I) \equiv \text{Max.}(R_1, R_2, R_3, R_4, R_5, R_6) , \tag{7.2}$$

where I is the number of the element. The maximum damage ratio, R_{\max} , for the entire laminate is obtained as

$$R_{\max} = \text{Max.}(R(I); I = 1, 2, 3, \dots, NE), \tag{7.3}$$

where NE is the number of elements. Therefore, by setting the applied stress $\sigma = 1/R_{\max}$, the computer program can tell the location of the initial damage zone and its mode of failure. For the analysis of the damage accumulation, the subsequent procedures could be described as follows:

Step 1: For a given set of input data, namely, the applied stress σ , the biaxial load factor k , the locations and the modes of failure of the damage zones, the element equation for each element, eqns. (5.9,5.10), and the final governing equation for the entire laminate will be obtained. Of course, the local stiffness matrix d'_{ij} of the damage zones should have been modified according to the modes of failure as indicated in the previous section.

Step 2: Solve the governing equation for the entire laminate and obtain the stress distribution for each element and its associated interface. For each element and its associated interface, compare the representative stresses with the failure strength and see whether any damage happens; if yes, change the stiffness matrix accordingly; otherwise, calculate the damage ratio, $R(I)$.

Step 3: Going through all the elements and their associated interfaces, if the damage zones are enlarged, keep the applied stress unchanged together with the enlarged damage zones and modes of failure as input data and go back to Step 1. Otherwise, calculate the maximum damage ratio, R_{\max} , and increase the applied stress by the factor $1/R_{\max}$ and go back to Step 1.

It is seen that there are two possibilities for a given applied stress, damage zones, and modes of failure. The first possibility is that the damage zones will not be enlarged and then that kind of damage is said to be localized at the applied stress specified. The second possibility is that the damage zones will be enlarged at a constant applied stress until the entire laminate is broken into pieces. In the second case, it is said that progressive failure occurs and the ultimate strength of the composite laminate is identified.

8. NUMERICAL RESULTS

First, let the input data relevant to this work be listed as follows:

1. Material constants:

$$\begin{aligned}
 E_L &= 134.58 \times 10^3 \text{ MPa} , \\
 E_T &= 9.68 \times 10^3 \text{ MPa} , \\
 \nu_{LT} &= 0.264 , \\
 \nu_{TZ} &= 0.435 , \\
 G_{LT} &= 4.48 \times 10^3 \text{ MPa} .
 \end{aligned}
 \tag{8.1}$$

2. Failure strength:

$$\begin{aligned}
 \sigma_{FN} &= 1241 \text{ MPa} , \\
 \sigma_{FS} &= 82.7 \text{ MPa} , \\
 \sigma_{MN} &= 55.2 \text{ MPa} , \\
 \sigma_{MS} &= 82.7 \text{ MPa} , \\
 \sigma_{DN} &= 55.2 \text{ MPa} , \\
 \sigma_{DS} &= 89.6 \text{ MPa} .
 \end{aligned}
 \tag{8.2}$$

3. Ply configuration:

$$[0,45,-45,90]_S = [90,-45,45,0,0,45,-45,90] . \tag{8.3}$$

4. Geometrical parameters:

$$\begin{aligned}
 2L &= 152.4 \text{ mm} , \\
 2W &= 152.4 \text{ mm} , \\
 2h &= 1.07 \text{ mm} , \\
 r_0 &= 12.7 \text{ mm} .
 \end{aligned}
 \tag{8.4}$$

5. Finite element mesh:

$$\begin{aligned}
 \text{No. of nodal points} &= 1750 , \\
 \text{No. of degrees of freedom} &= 5250 , \\
 \text{No. of elements} &= 1248 , \\
 \text{Volume of smallest element} &= 0.175 \text{ mm}^3 .
 \end{aligned}
 \tag{8.5}$$

For illustrative purpose, the numerical results of three cases, $k = 0, 0.5, 1$, are presented as follows:

Case 1: uniaxial loading, $k = 0$

The maximum tensile stress along the fiber among the top four layers, $\max. \sigma_L$, is plotted in Fig. 6 as a function of θ at $r = 13.1 \text{ mm}$. It is noticed that the overall $\max. \sigma_L$ occurs at $\theta = 0^\circ (180^\circ)$ in the fourth layer in which the fibers are parallel to the y-axis--the loading direction and the maximum stress concentration factor is as high as 7.92, which means the fourth layer carries the major portion of the load.

The maximum normal stress perpendicular to the fiber among the top four layers, $\max. \sigma_T$, is plotted in Fig. 7 as a function of θ at $r = 13.1$ mm. It is noticed that the overall $\max. \sigma_T (= 0.56\sigma)$ occurs at $\theta = 172.5^\circ (-7.5^\circ)$ in the first layer, which indicates the first damage zone of matrix failure will be initiated in the element of the first layer centered at $r = 13.1$ mm and $\theta = 172.5^\circ (-7.5^\circ)$ when the applied stress σ reaches 98.6 MPa (Fig. 8). At $\sigma = 138$ MPa, the damage zone is shown in Fig. 9. However, those damages are localized, which means that the damage zone will not be enlarged if the applied stress is not increased further. At $\sigma = 156$ MPa, the first fiber breakage occurs in the element of the fourth layer centered at $r = 13.1$ mm and $\theta = 0^\circ (180^\circ)$ as shown in Fig. 10 and that leads to progressive failure as indicated by Fig. 11 and Fig. 12. In this case, the ultimate strength of the composite laminate is identified to be 156 MPa.

Case 2: Biaxial loading, $k = 0.5$

Similarly, $\max. \sigma_L$ and $\max. \sigma_T$ are plotted as functions of θ at $r = 13.1$ mm in Fig. 13 and Fig. 14, respectively. Again, the overall $\max. \sigma_L$ occurs at $\theta = 0^\circ (180^\circ)$ in the fourth layer but the maximum stress concentration factor is reduced to 6.57 due to the load

applied parallel to the x-axis. The overall max. σ_T ($= 0.466\sigma$) occurs at $\theta = 172.5^\circ$ (-7.5°) in the first layer, which means the first matrix failure will happen when the applied stress σ reaches 119 MPa (Fig. 15). The damage zone at $\sigma = 175$ MPa is shown in Fig. 16. At $\sigma = 189$ MPa, fiber breakage occurs and that leads to progressive failure as indicated by Figs. 17,18; thus, the ultimate strength in this case is obtained to be 189 MPa.

Case 3: Equal biaxial loading, $k = 1$

The maximum tensile stress along the fiber among the top four layers, max. σ_L , plotted in Fig. 19 as a function of θ , is noticed to have four peak values - 5.226σ , 5.252σ , 5.214σ , 5.245σ - at $\theta = 0^\circ$ (180°), 45° (225°), 90° (270°), 135° (315°), respectively. This means that, first, the maximum stress concentration factor is further reduced to the neighborhood of 5.2 and, second, the final broken path of the specimen may be one of the four lines: $\theta = 0^\circ$ - 180° , 45° - 225° , 90° - 270° , 135° - 315° . Figure 20, which shows max. σ_T as a function of θ , indicates that the overall max. σ_T ($= 0.382\sigma$) occurs at $\theta = 165^\circ$ (-15°) in the first layer. This means the first matrix failure will happen when the applied stress σ reaches 144 MPa (Fig. 21).

The damage zones at $\sigma = 172$ MPa and at $\sigma = 192$ MPa are shown in Fig. 22 and Fig. 23, respectively and it is noticed that those damages are localized. At $\sigma = 193$ MPa, fiber breakage occurs and that leads to progressive failure as indicated in Figs. 24,25; thus, the ultimate strength in the equal biaxial loading case is obtained as 193 MPa.

9. DISCUSSIONS

This three dimensional finite element computer program can be used to calculate the six components of stress $\sigma_x, \sigma_y, \sigma_z, \sigma_{yz}, \sigma_{zx}, \sigma_{xy}$ (or equivalently, $\sigma_L, \sigma_T, \sigma_z, \sigma_{LS}, \sigma_{TS}, \sigma_{zS}$) at any point in the composite laminate. Based on this stress distribution and the given failure criterion, the damage zones and the modes of failure can be identified. According to the modes of failure, the stiffness matrix of those elements in the damage zones will be modified and then subsequently the new stress distribution is obtained. This new stress distribution determines the enlargement of the damage zones or the higher load which the composite laminate is able to carry. This process can go on and on until progressive failure occurs and therefore the ultimate strength of the composite laminate is obtained.

From the three cases presented in the previous section, it is noticed that: (1) the initial stress distribution of σ_T near the edge of the hole determines the location of initial damage zone and its mode of failure as well as the applied stress for initial damage; (2) the initial stress distribution of σ_L near the edge of the hole predicts the final broken path of the specimen.

It has also been noticed that, during the whole process of damage enlargement and progressive failure, the computer

program has never detected any delamination. Many authors, including Spilker and Chou [13], Altus et al. [14], Raju and Crews [15], have investigated the free edge effects in composite laminate and reported that both normal stress and shear stress between two composite layers have singularities near the free edge and therefore, logically, delamination should happen prior to the occurrence of other modes of failure. This program's failure to detect the occurrence of delamination is most likely due to the coarseness, relatively speaking, of the finite element mesh near the edge of the hole. However, further refinement of the finite element mesh to the required level at this stage is practically impossible and, hence, additional effort and a new approach will be necessary in this respect.

Acknowledgement -- The author wishes to acknowledge the financial support for this work from NASA-Langley Research Center (Grant NSG 1289). The author also wishes to express deep gratitude to Dr. Harold Liebowitz for his valuable suggestions, helpful discussions, and enthusiastic encouragement.

REFERENCES

1. Mechanics of Composite Materials, Proc. of the 5th Symposium on Naval Structural Mechanics (Edited by F.W. Wendt, H. Liebowitz and N. Perrone), Pergamon Press, Oxford (1970).
2. L.R. Calcote, The Analysis of Laminated Composite Structures, Von Nostrand Reinhold Company, New York (1969).
3. S.K. Garg, V. Svalbonas and G.A. Gurtman, Analysis of Structural Composite Materials, Marcel Dekker, New York (1973).
4. Composite Materials, Structural Design and Analysis, Part 1 and 2, (Edited by C.C. Chamis), Academic Press, New York (1975).
5. R.M. Jones, Mechanics of Composite Materials, McGraw-Hill, New York (1975).
6. S.S. Wang, J.F. Mandell and F.J. McGarry, "Three Dimensional Solution for a Through-Thickness Crack in a Crossplied Laminate," "Three Dimensional Solution for a Through-Thickness Crack with Crack Tip Damage in a Crossplied Laminate," "A Multilayer Hybrid-Stress Finite Element Analysis of a Through-Thickness Edge Crack in a $\pm 45^\circ$ Laminate," and "Fracture of Fiber Reinforced Composites," Research Report R 76- 5,6,7,8, School of Engineering, Massachusetts Institute of Technology (1976).
7. A.K. Noor and C.M. Anderson, "Mixed Isoparametric Finite Element Models of Laminated Composite Shells," Computer Methods in Applied Mechanics and Engineering, 11 (3), 225 (1977).
8. W.P. Witt, III, A.N. Palazotto and H.T. Hahn, "Numerical and Experimental Comparison of the Notch Tip Stresses in a Laminated Plate," AIAA Journal, 17, 500 (1979).
9. T. Nishioka and S.N. Atluri, "Assumed Stress Finite Element Analysis of Through-Cracks in Angle-Ply Laminates," AIAA Journal, 18, 1125 (1980).
10. J.D. Lee, "Three Dimensional Finite Element Analysis of Layered Fiber-Reinforced Composite Materials," Computers & Structures, 12, 319 (1980).

11. A.C. Eringen, Mechanics of Continua, Wiley, New York (1967).
12. L.J. Segerlind, Applied Finite Element Analysis, Wiley, New York (1976).
13. R.L. Spilker and S.C. Chou, "Edge Effects in Symmetric Composite Laminate: Importance of Satisfying the Traction-Free-Edge Condition," J. Composite Materials, 14, 2 (1980).
14. E. Altus, A. Rotem, and M. Shmueli, "Free Edge Effect in Angle Ply Laminates - A New Three Dimensional Finite Difference Solution," J. Composite Materials, 14, 21 (1980).
15. I.S. Raju and J.H. Crews, Jr., "Interlaminar Stress Singularities at a Straight Free Edge in Composite Laminate," Computers & Structures, 14, 21 (1981).

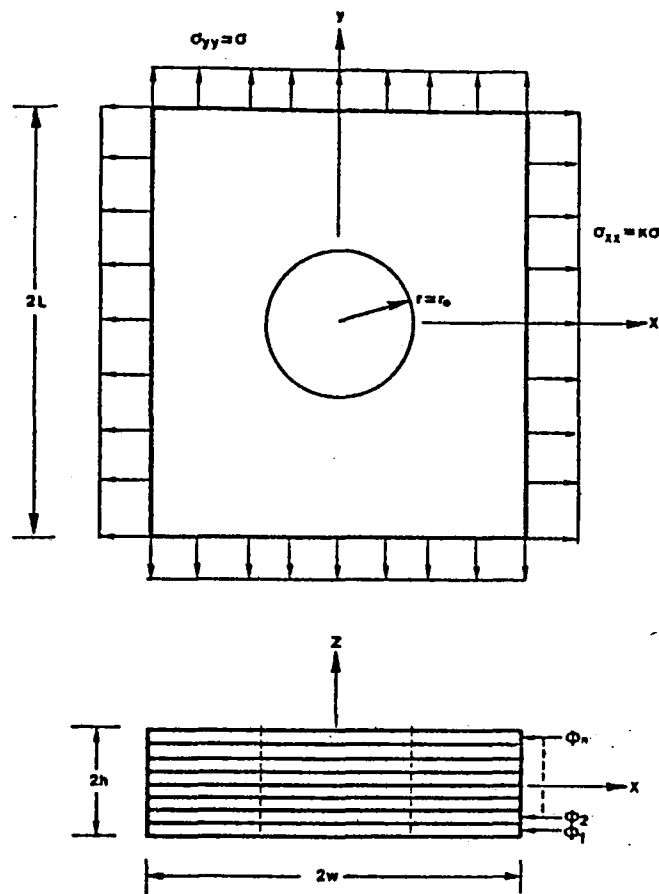


FIG. 1 THE TOP VIEW AND THE FRONT VIEW OF A COMPOSITE LAMINATE

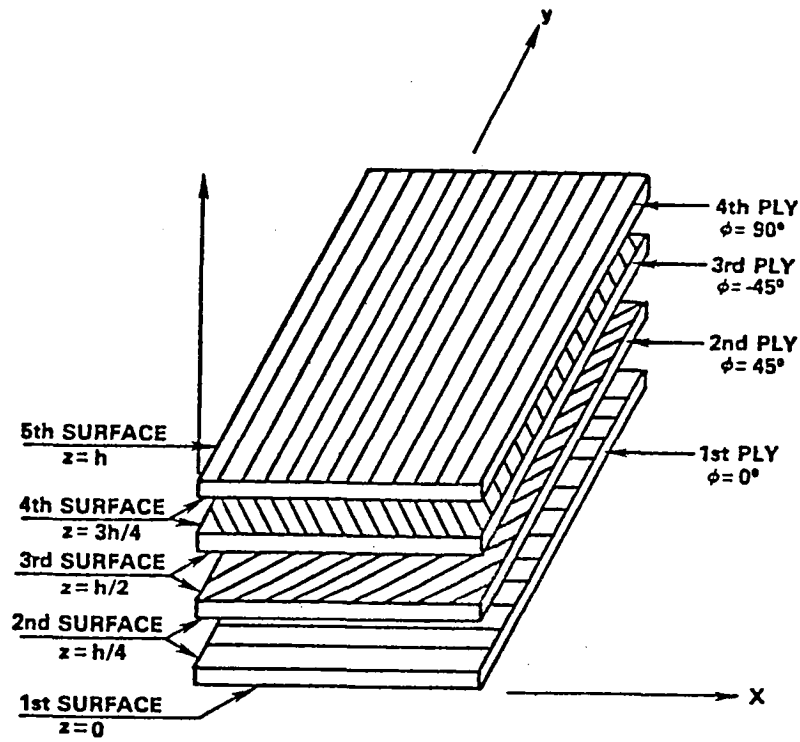


FIG. 2 THE TOP FOUR PLIES OF A SYMMETRIC PLY CONFIGURATION
 $(0, 45, -45, 90)_s$

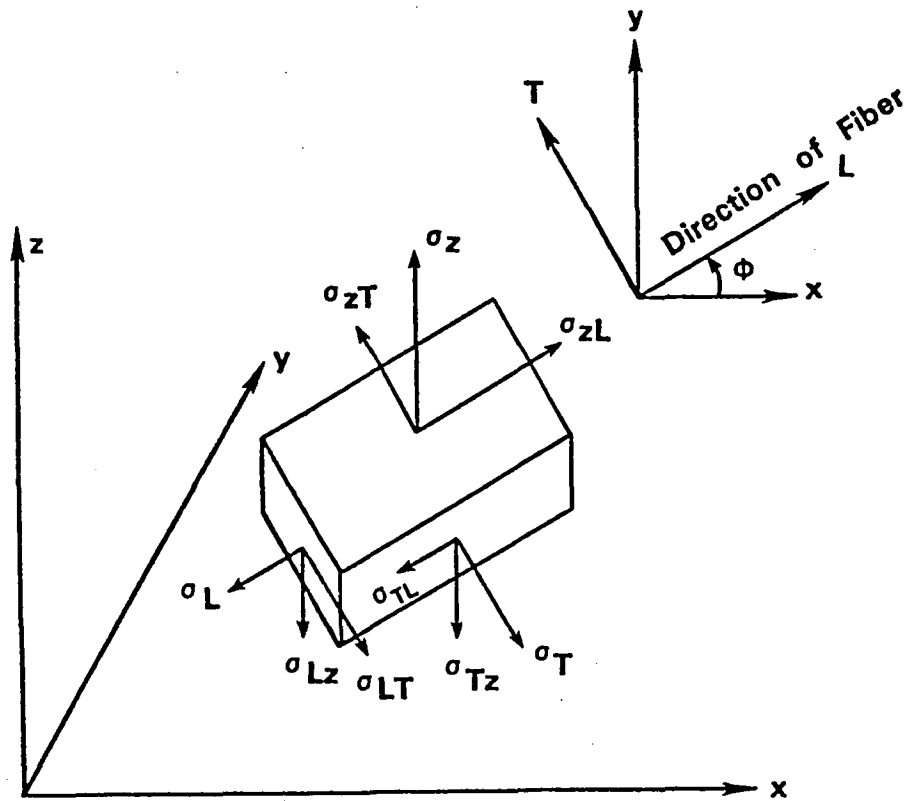


Fig.3 The Stress Components in (L, T, z) Coordinate System

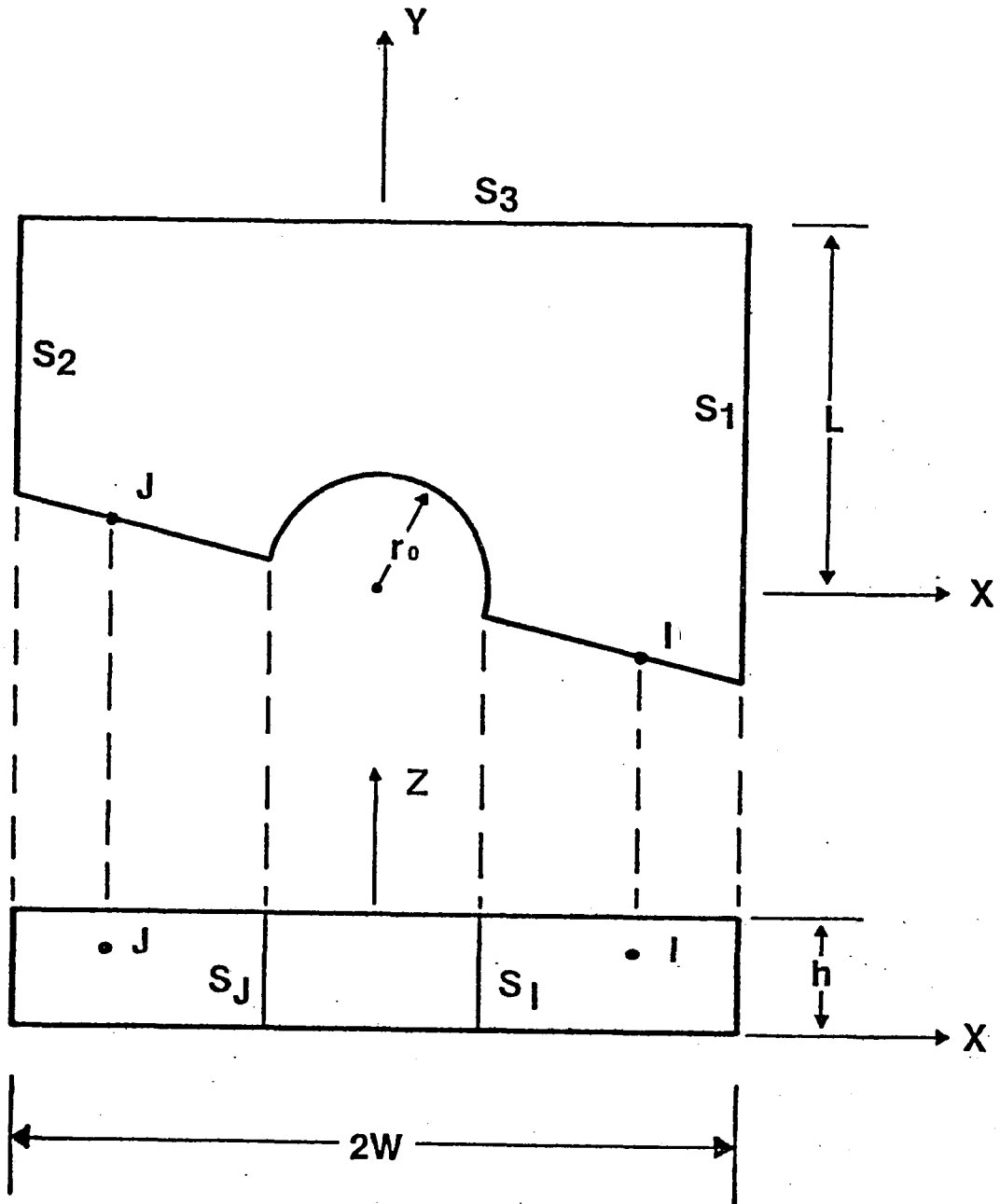


Fig. 4 A Quarter of the Laminate

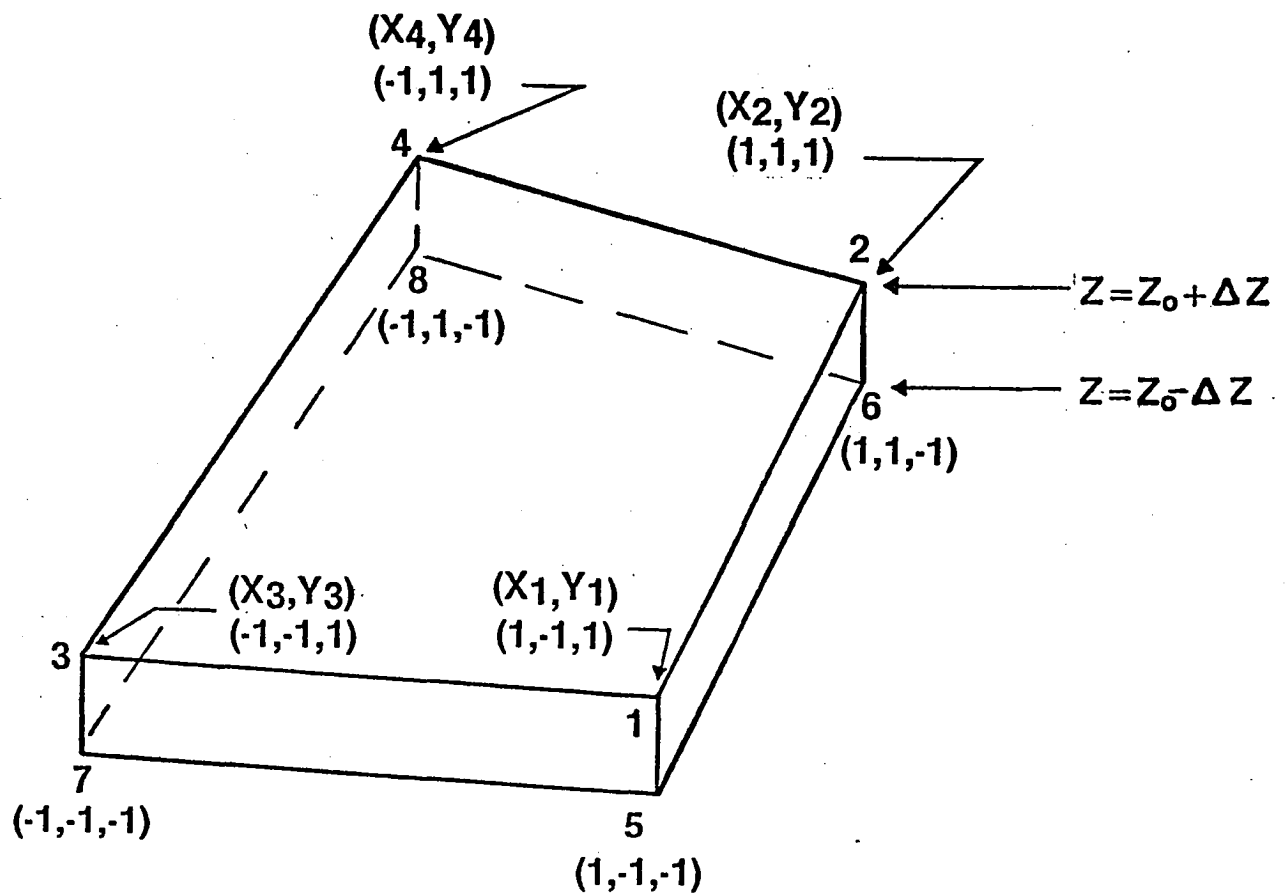


Fig. 5 A Typical 8-Node Element

MAX. σ_L/σ

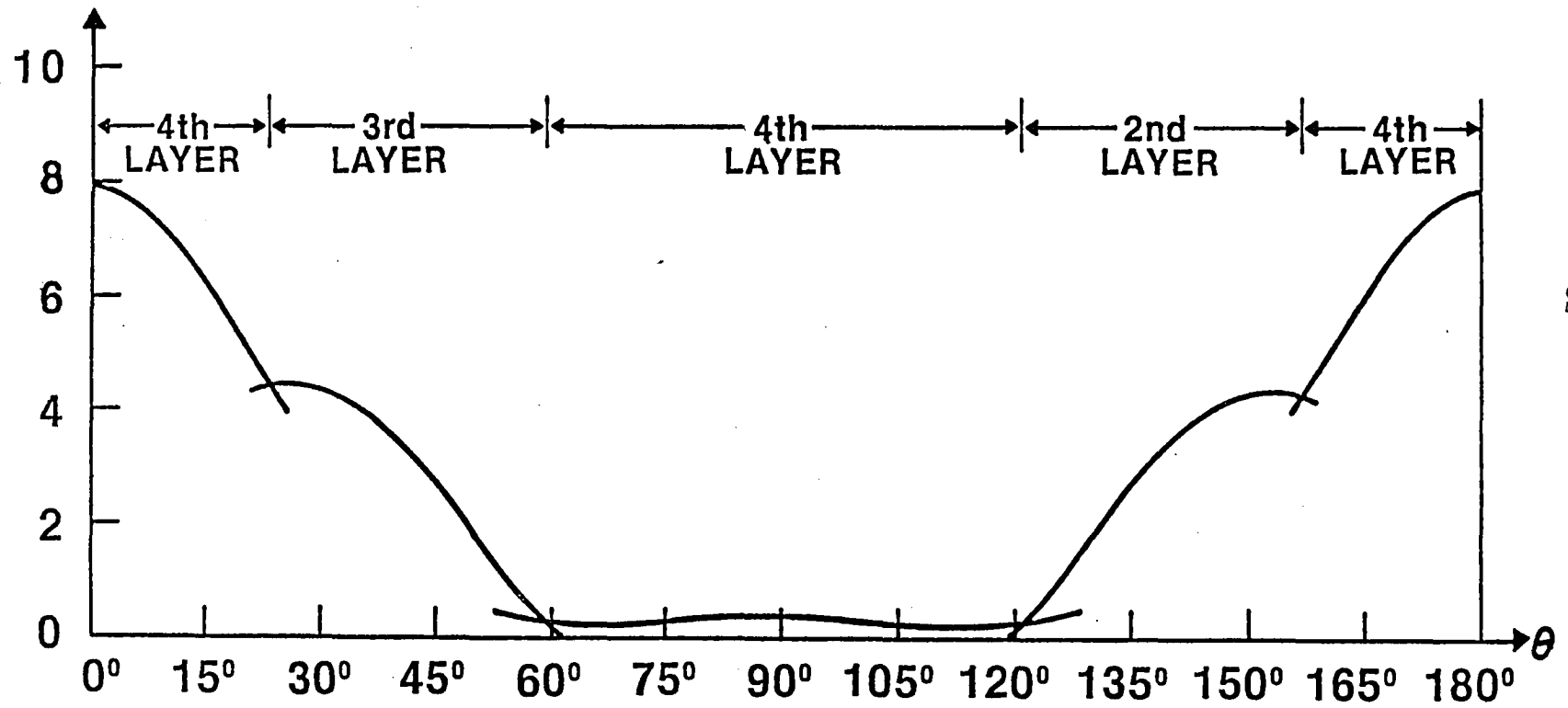


Fig. 6. MAX. σ_L vs θ at $r = 13.1 \text{ mm.}$, $k = 0$

MAX. σ_T/σ

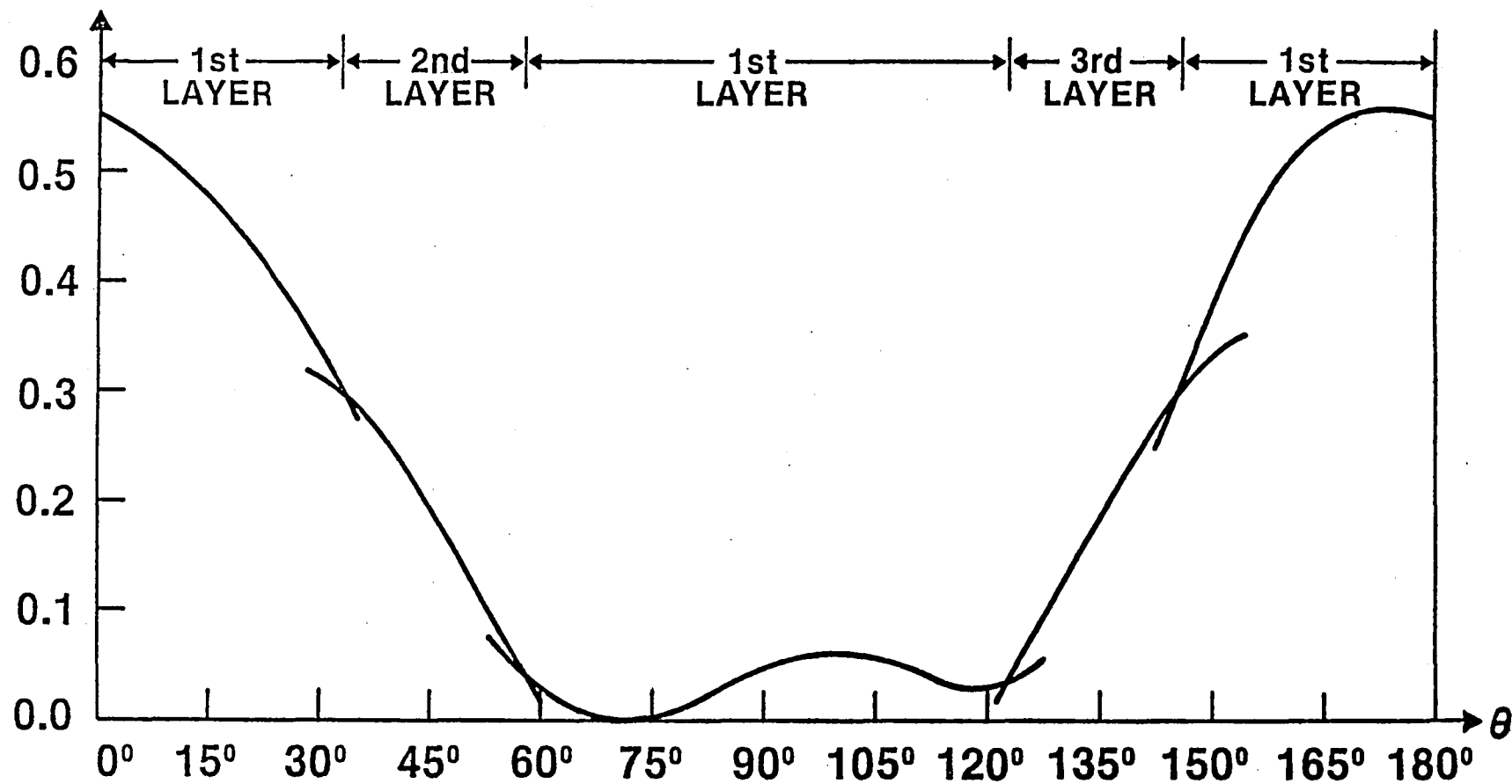


Fig. 7. MAX. σ_T vs θ at $r = 13.1\text{mm.}$, $k = 0$

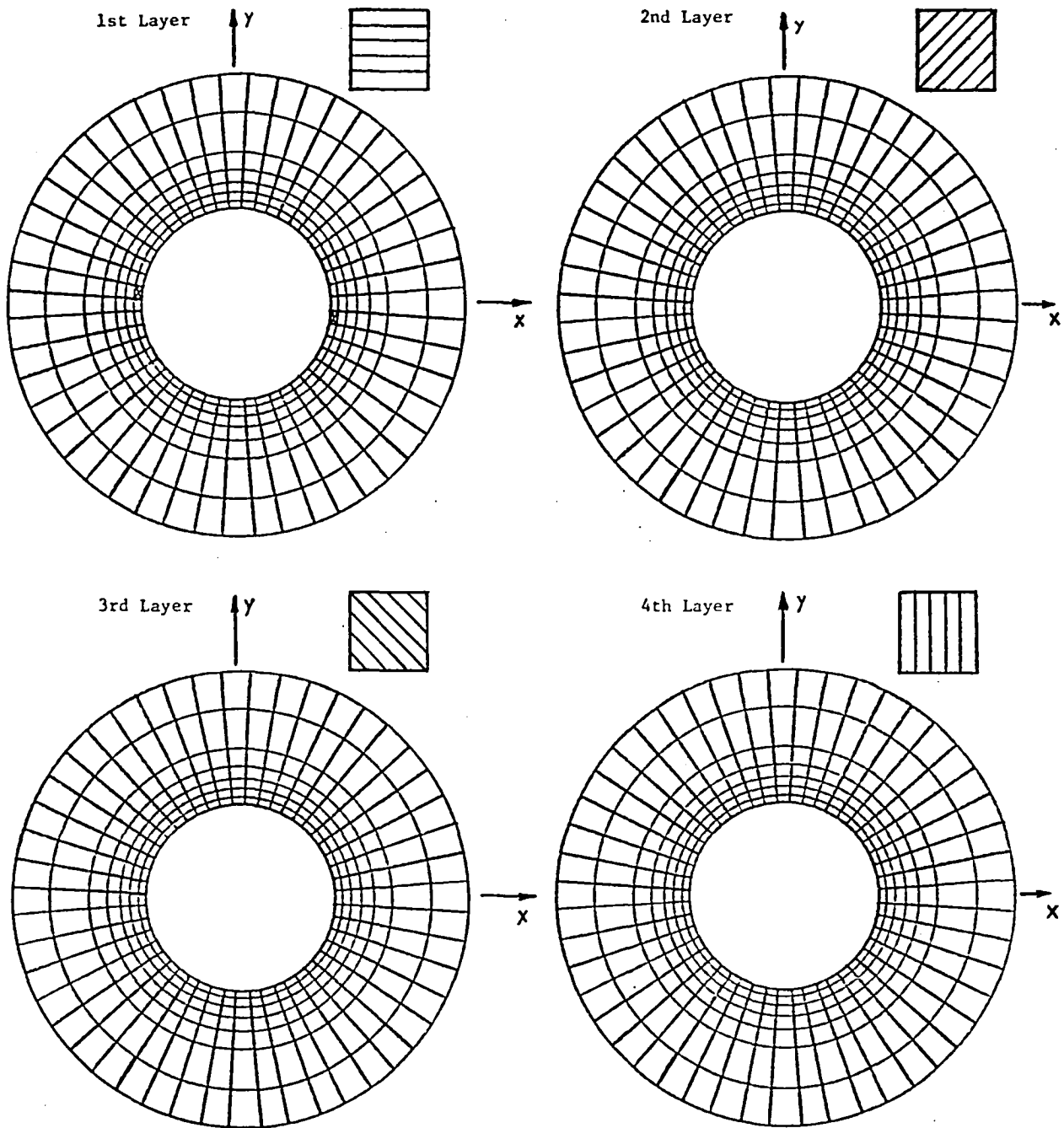


Fig. 8. Damage zone at $\sigma = 98.6$ MPa, $k = 0$. Matrix Failure \boxtimes Fiber Breakage \blacksquare

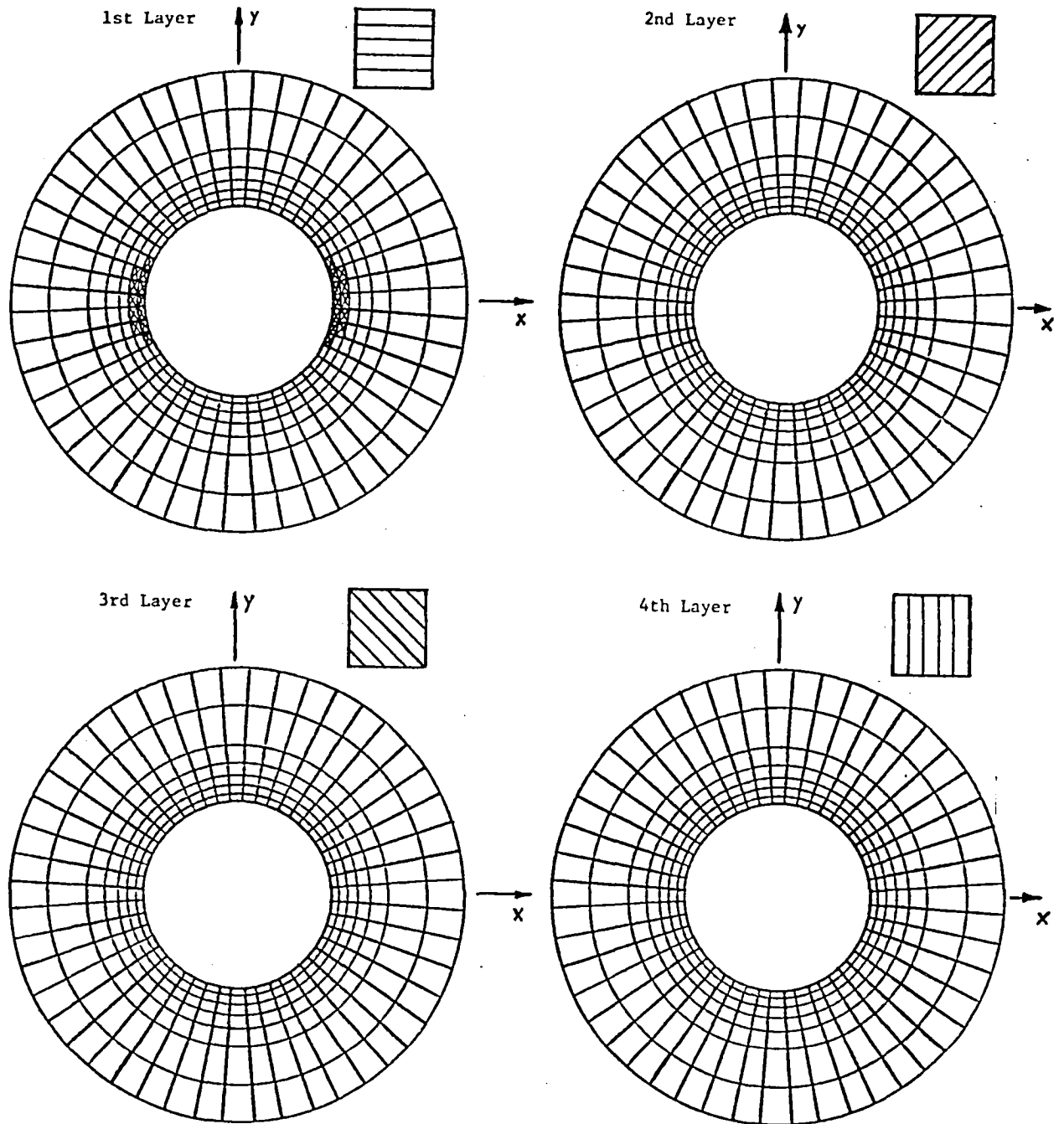




Fig. 9. Damage zone at $\sigma = 138$ MPa, $k = 0$. Matrix Failure  Fiber Breakage 

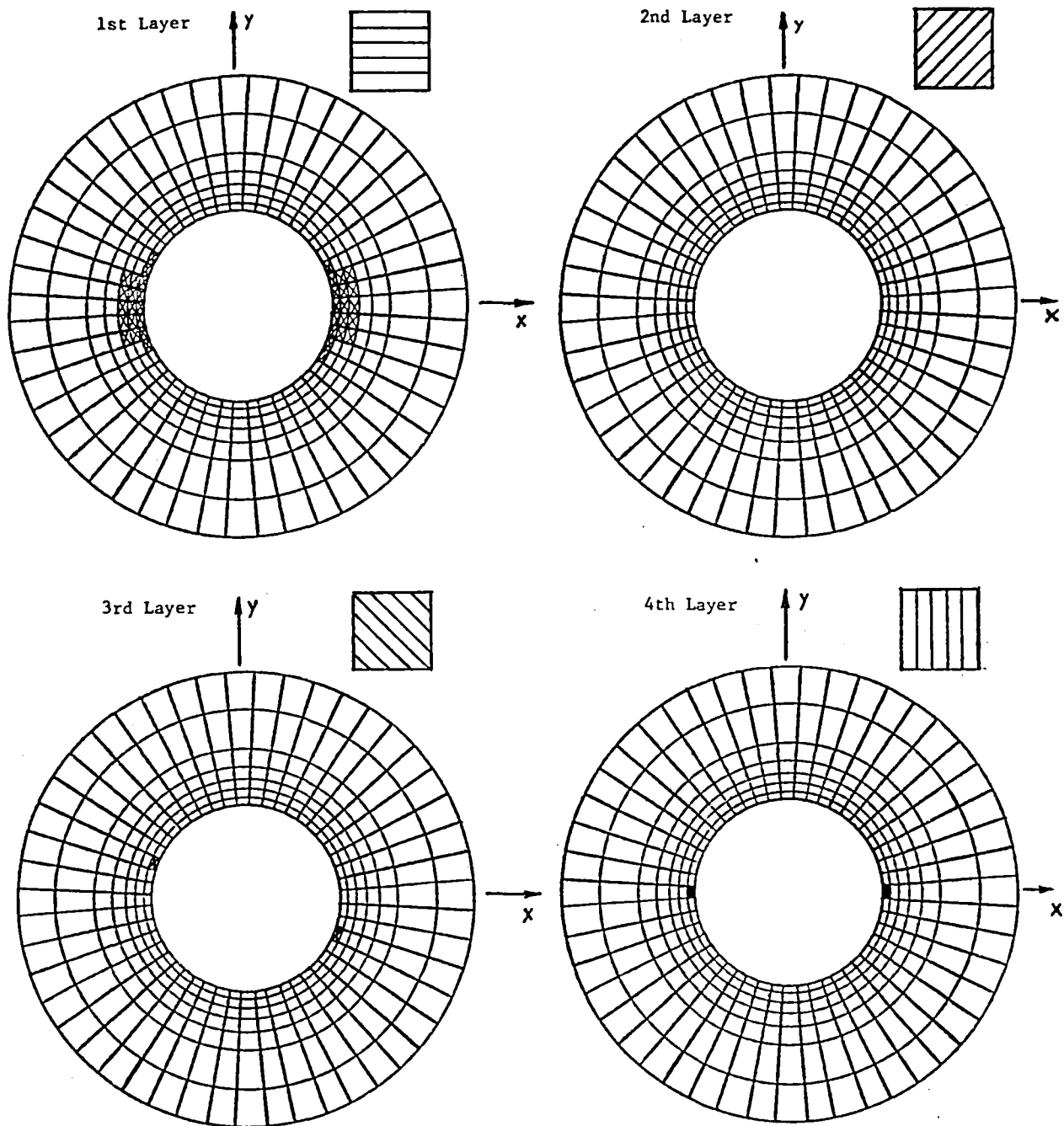


Fig. 10. Damage zone at $\sigma = 156$ MPa, $k = 0$. Matrix Failure \boxtimes Fiber Breakage \blacksquare

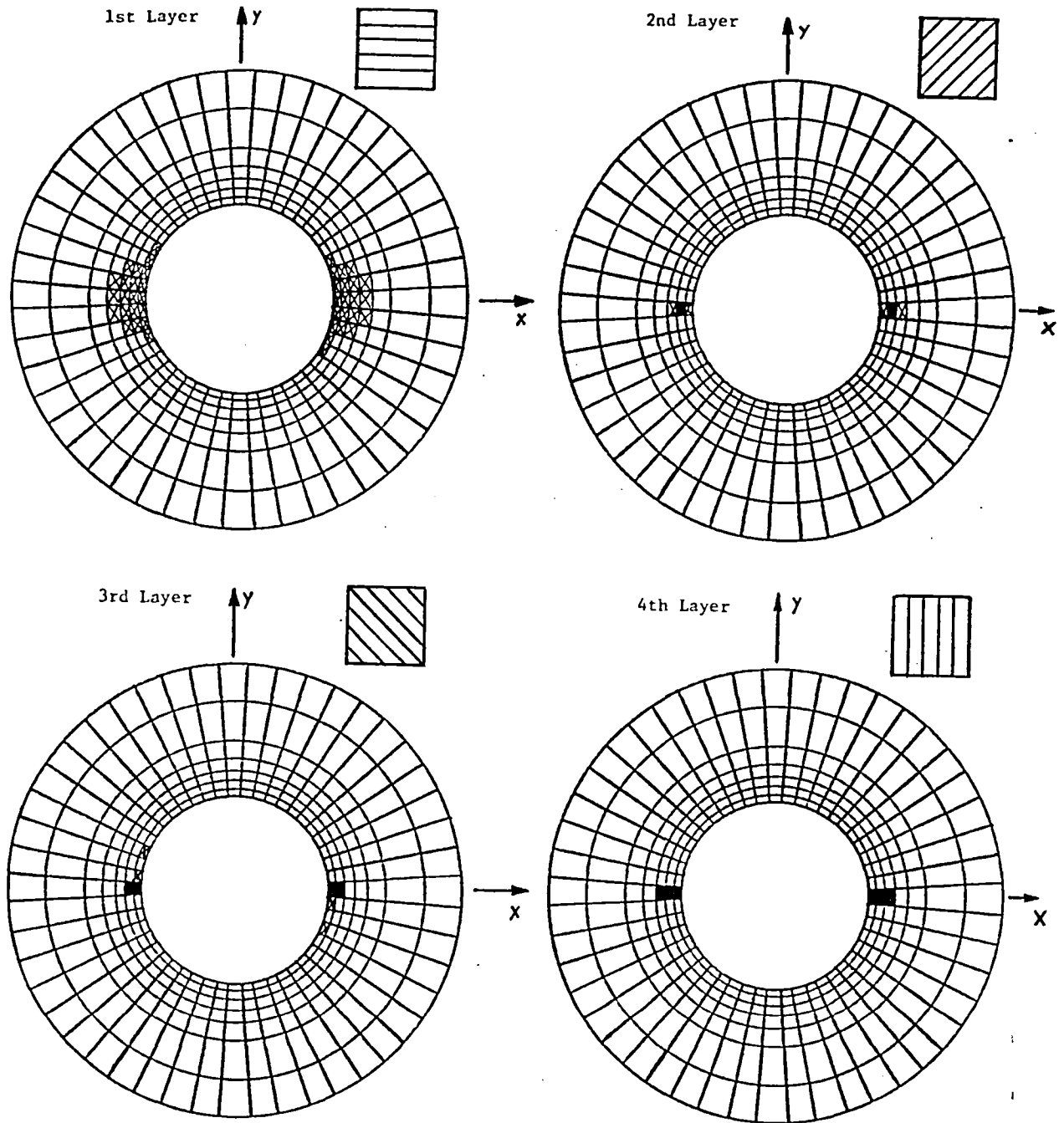


Fig. 11. Damage zone at $\sigma = 156$ MPa, $k = 0$. Matrix Failure \boxtimes Fiber Breakage \blacksquare

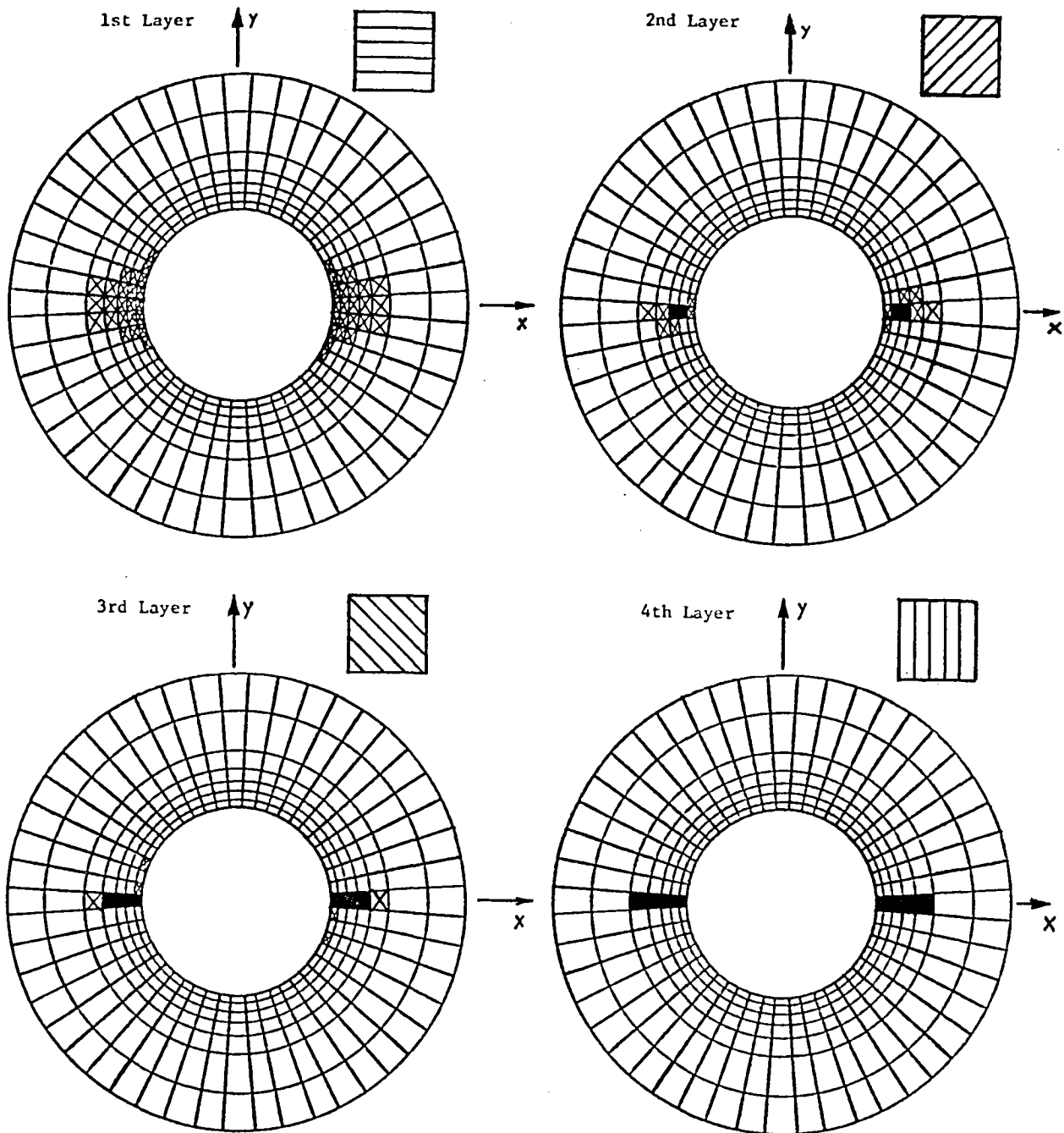


Fig. 12. Damage zone at $\sigma = 156$ MPa, $k = 0$. Matrix Failure \otimes Fiber Breakage \blacksquare

MAX. σ_L / σ

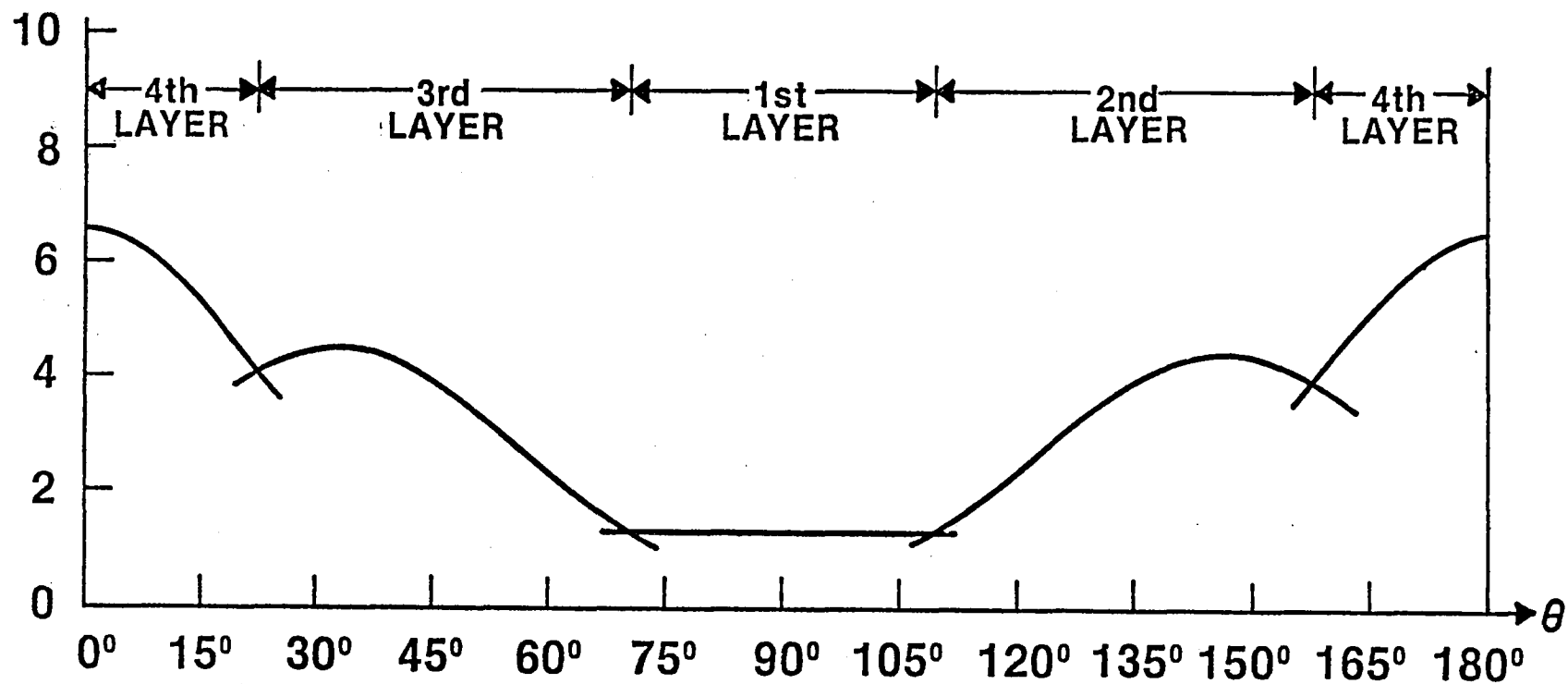


Fig. 13. MAX. σ_L vs θ at $r = 13.1$ mm, $k = 0.5$

MAX. σ_T/σ

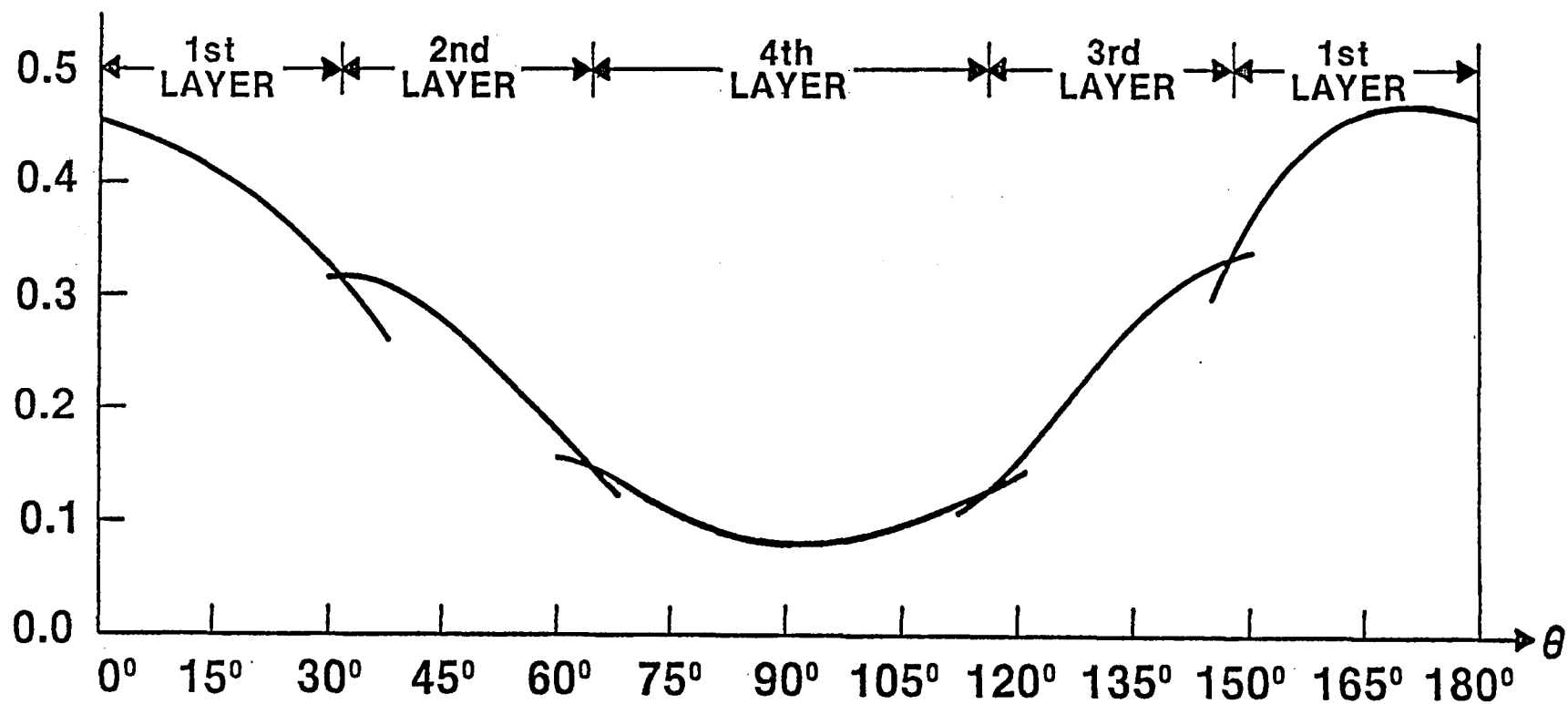


Fig. 14. MAX. σ_T vs θ at $r = 13.1$ mm, $k = 0.5$

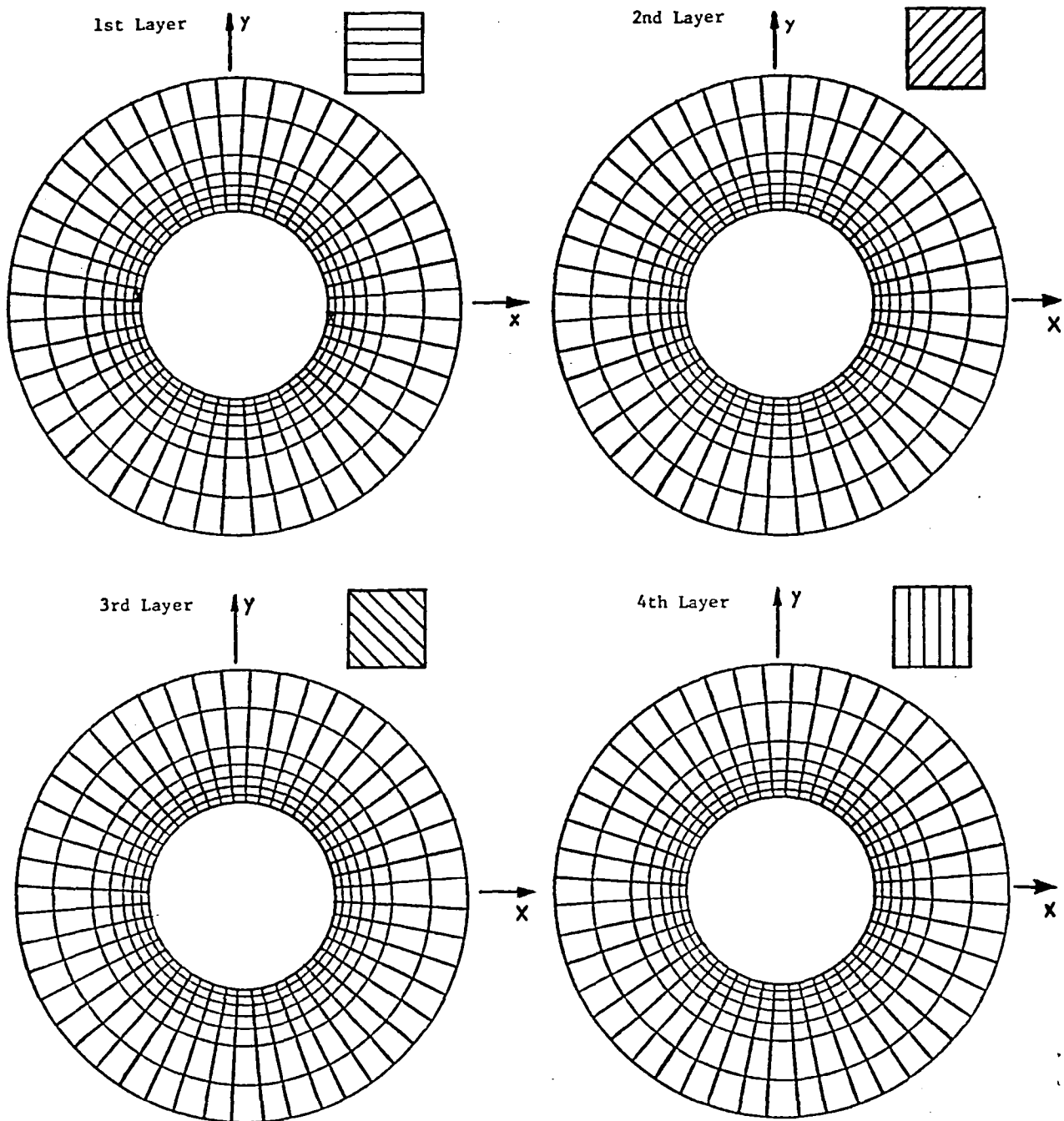




Fig. 15. Damage zone at $\sigma = 119$ MPa, $k = 0$. Matrix Failure  Fiber Breakage 

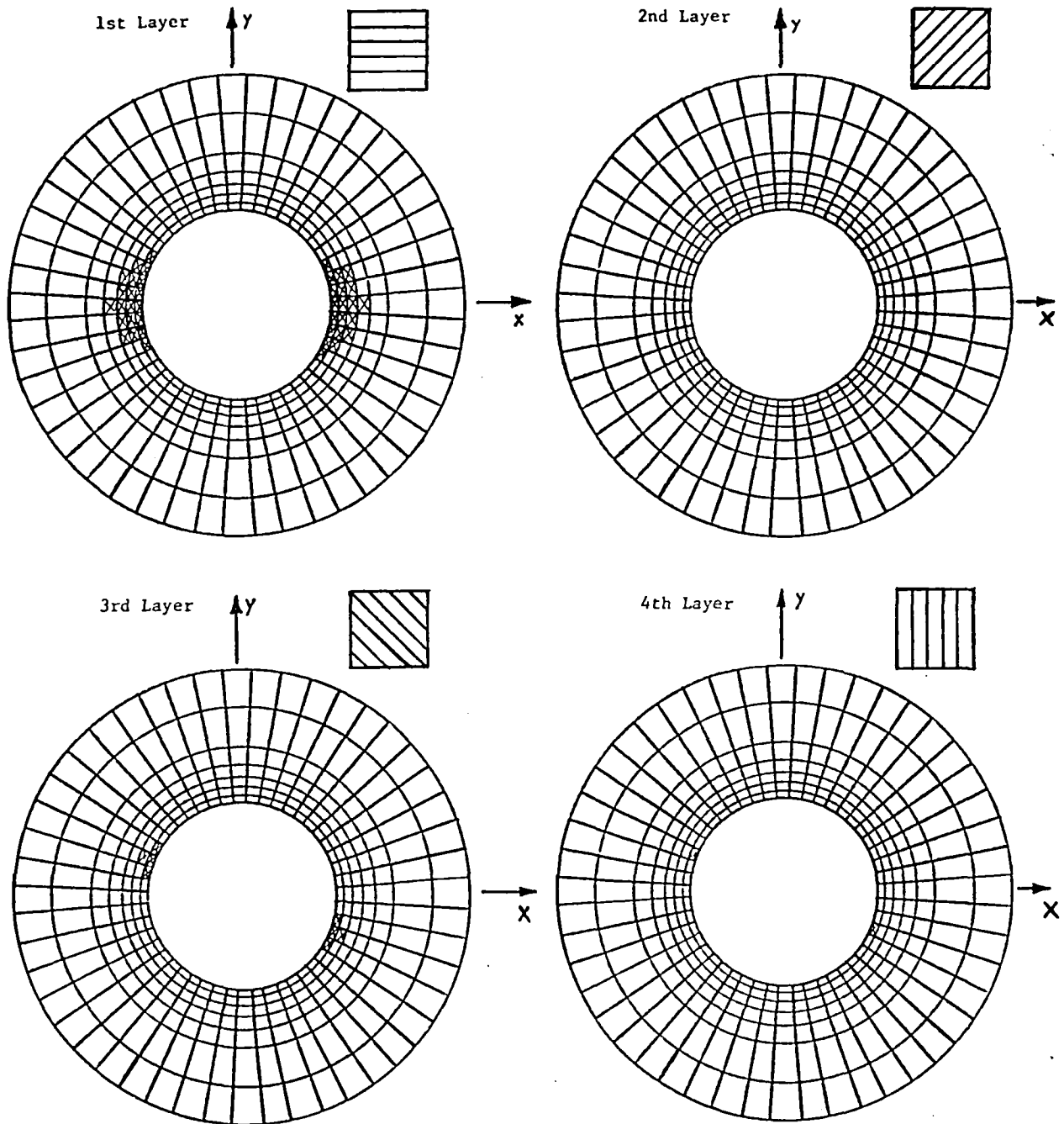


Fig. 16. Damage zone at $\sigma = 175$ MPa, $k = 0.5$. Matrix Failure \boxtimes Fiber Breakage \blacksquare

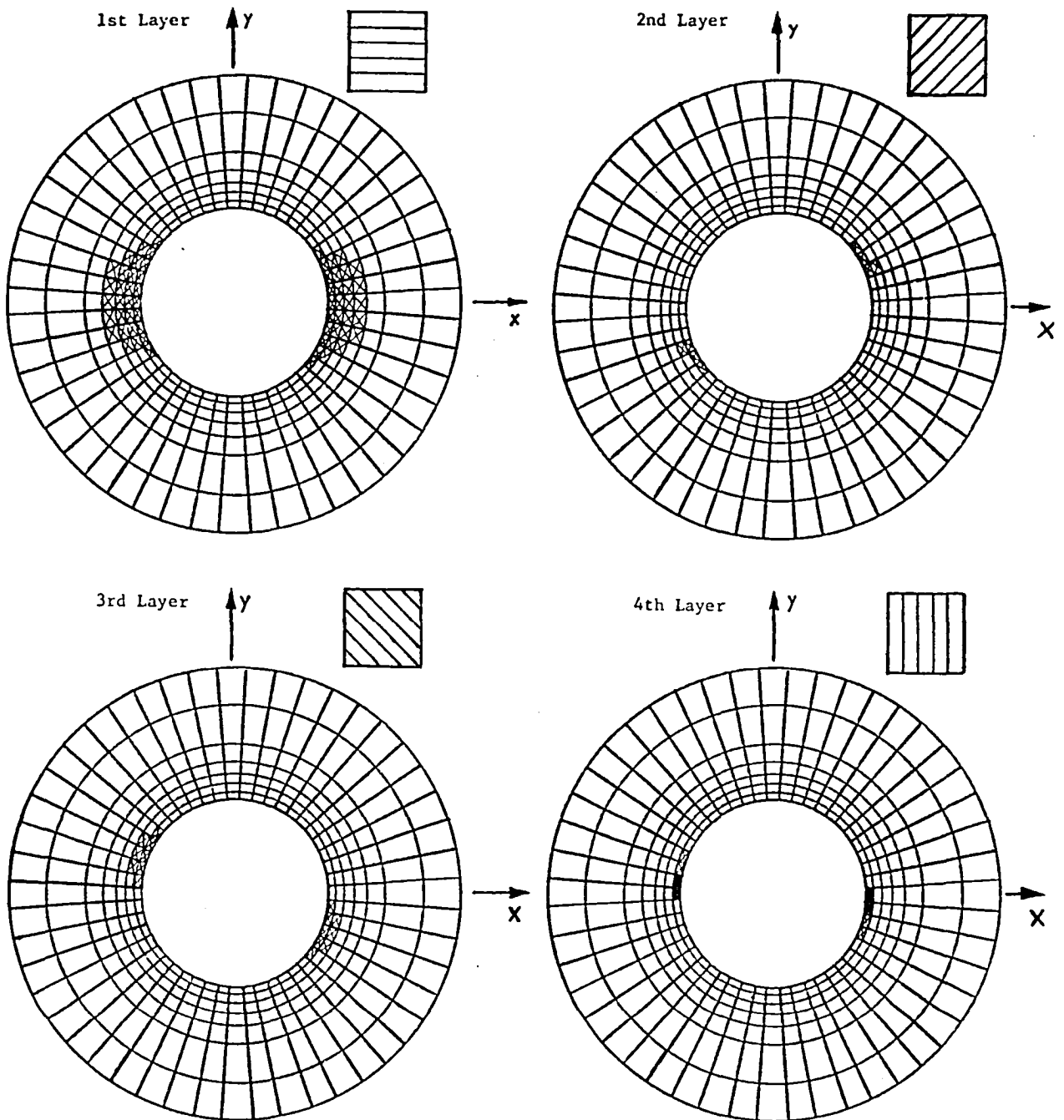


Fig. 17. Damage zone at $\sigma = 189$ MPa, $k = 0.5$. Matrix Failure \otimes Fiber Breakage \blacksquare

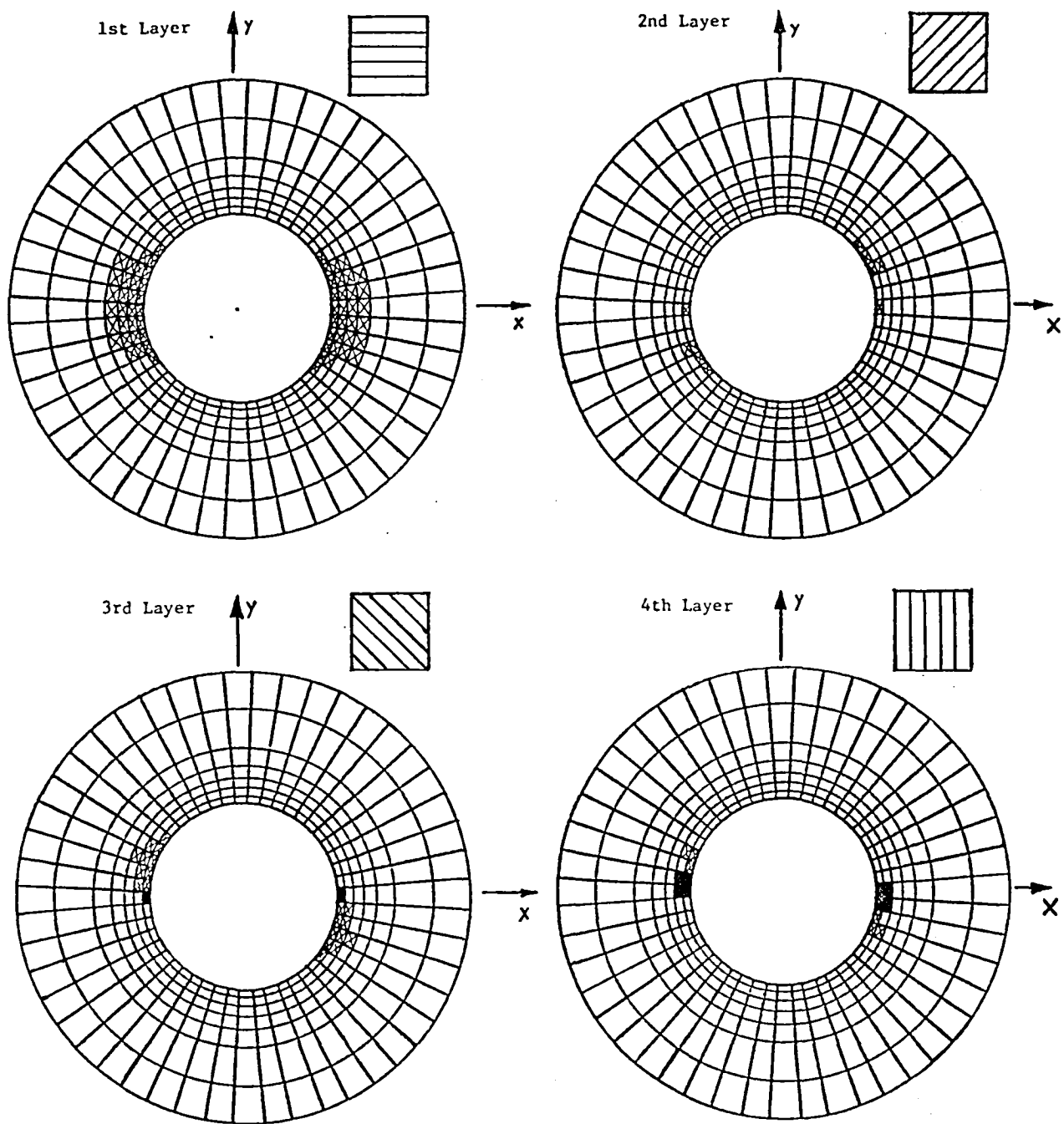




Fig. 18. Damage zone at $\sigma = 189$ MPa, $k = 0.5$. Matrix Failure  Fiber Breakage 

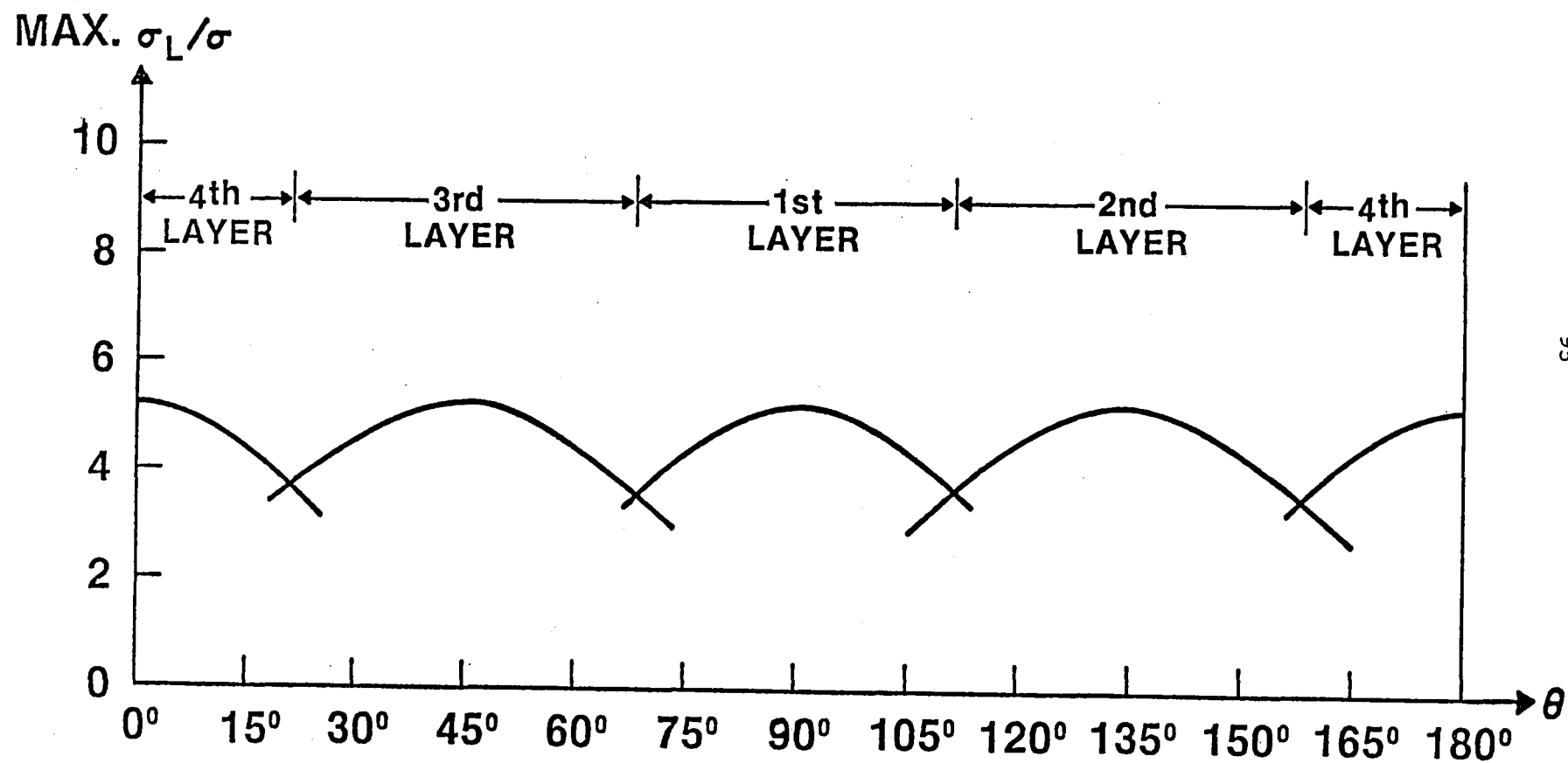


Fig. 19. MAX. σ_L vs θ at $r = 13.1$ mm, $k = 1$

MAX. σ_T / σ

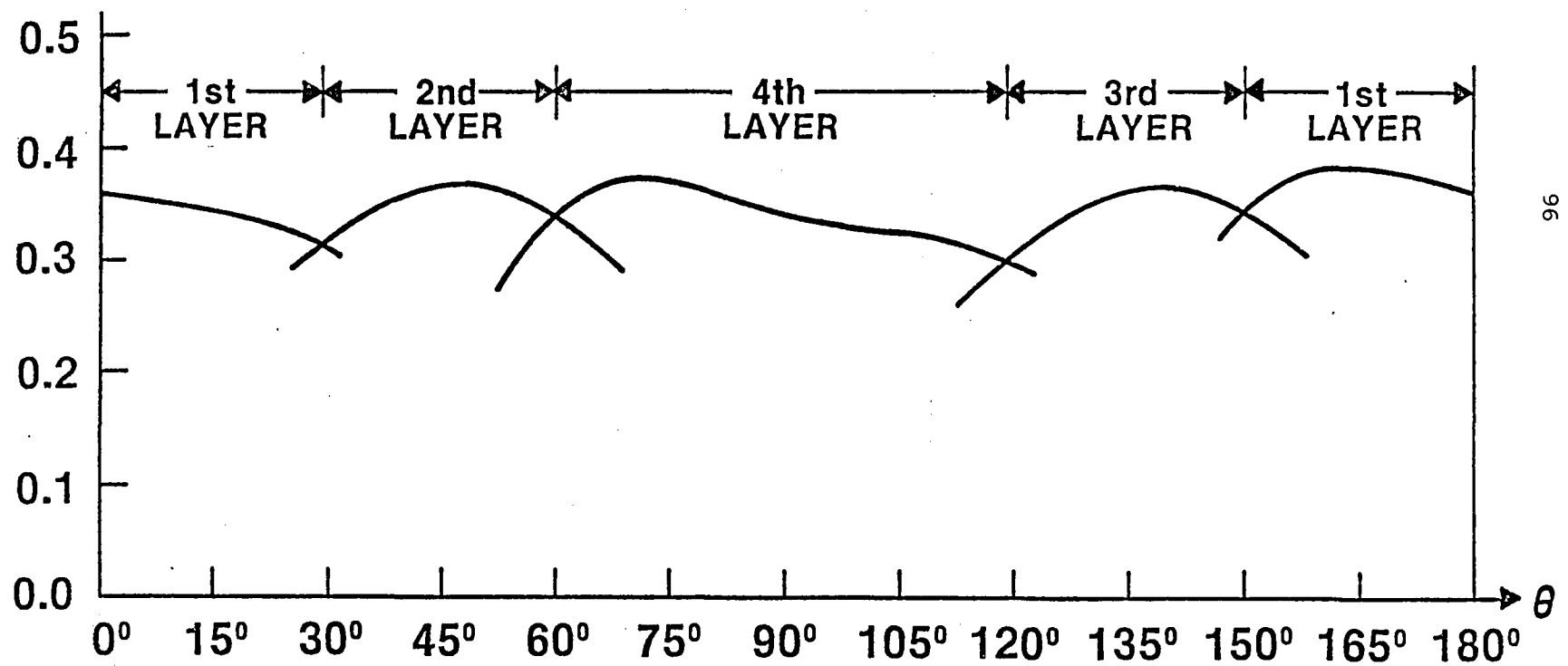


Fig. 20. MAX. σ_T vs θ at $r = 13.1$ mm, $k = 1$

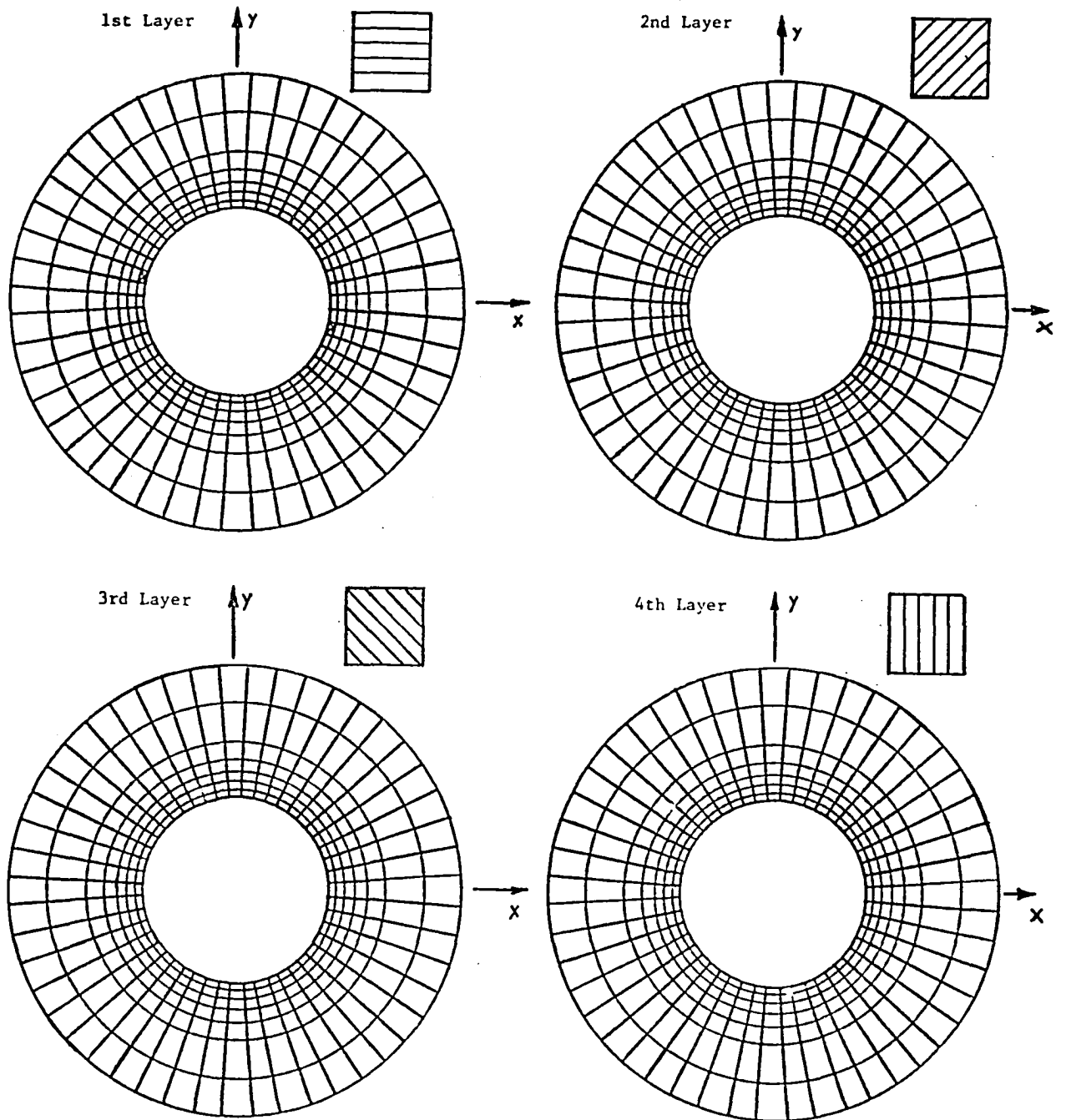




Fig. 21. Damage zone at $\sigma = 144$ MPa, $k = 0$. Matrix Failure  Fiber Breakage 

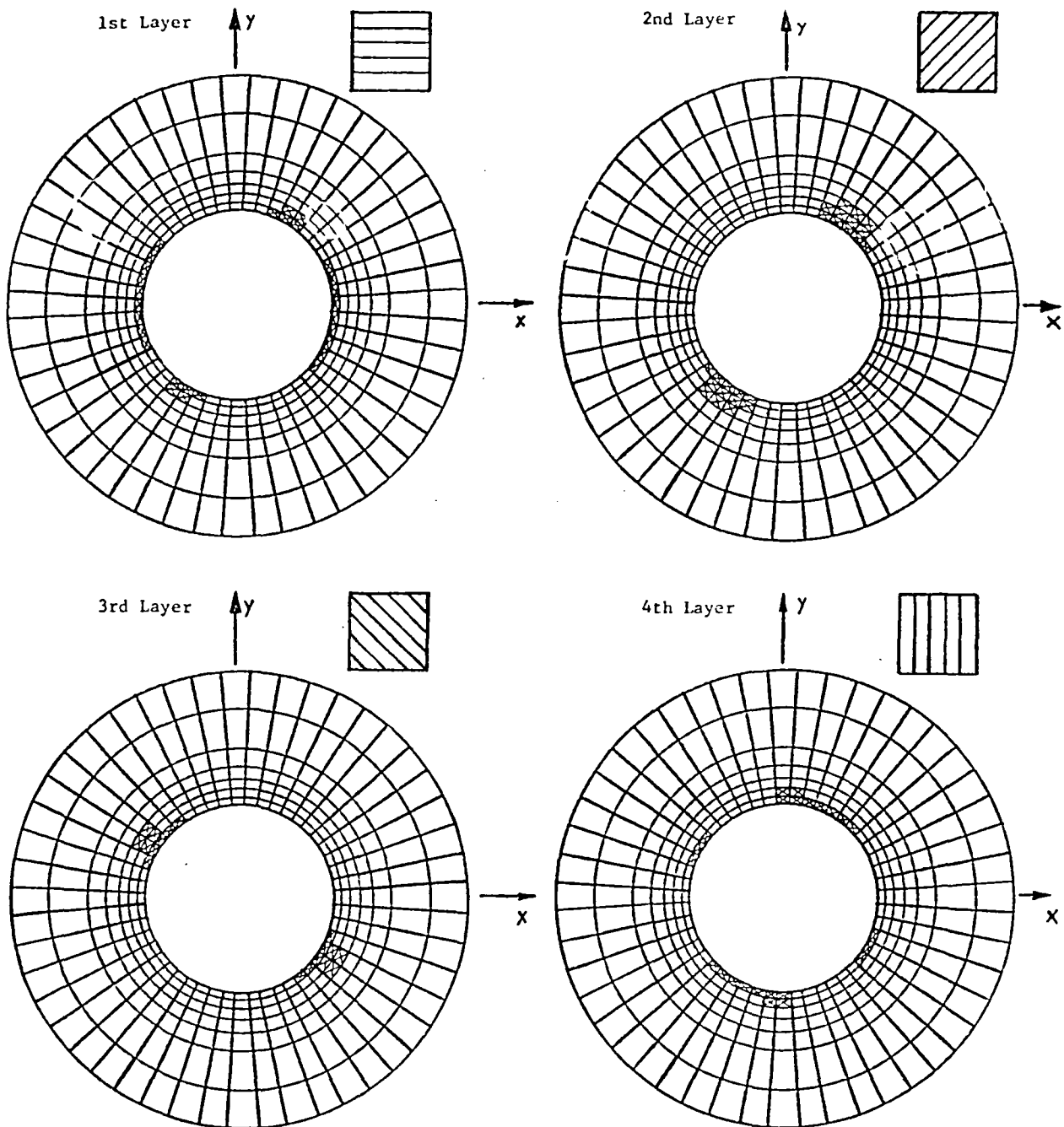




Fig. 22. Damage zone at $\sigma = 172$ MPa, $k = 0$. Matrix Failure  Fiber Breakage 

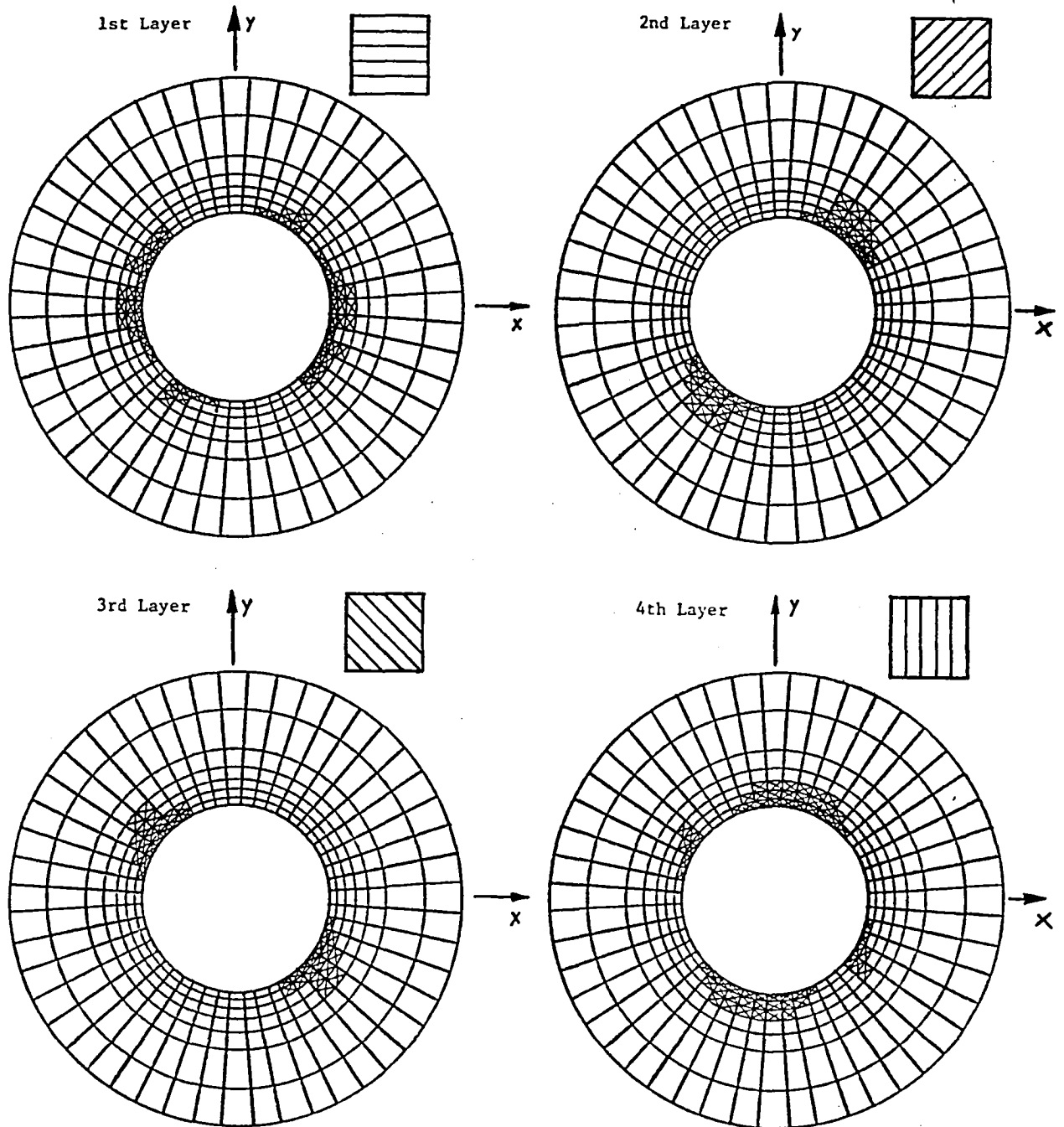




Fig. 23. Damage zone at $\sigma = 192$ MPa, $k = 0$. Matrix Failure  Fiber Breakage 

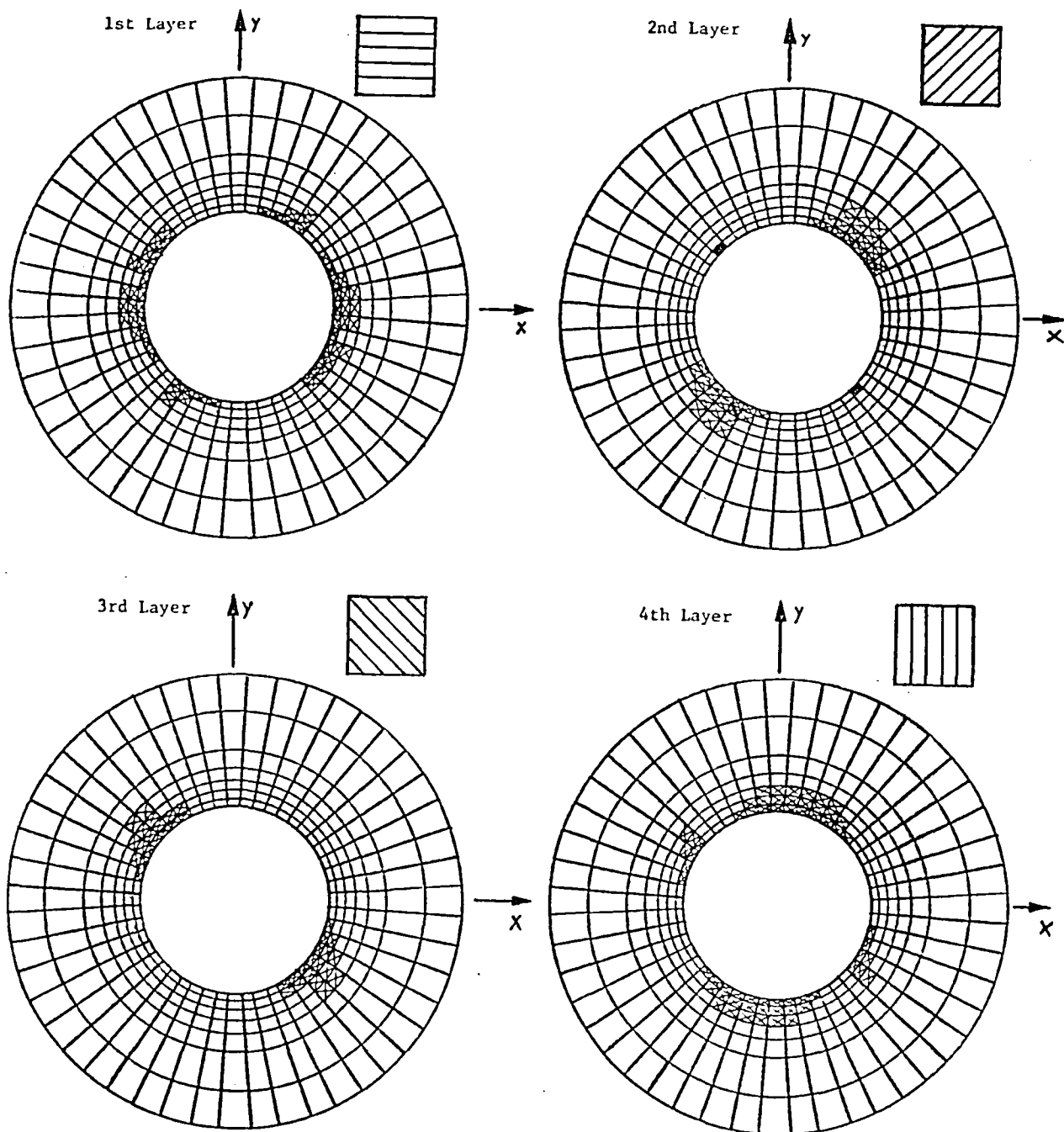


Fig. 24. Damage zone at $\sigma = 193$ MPa, $k = 0$. Matrix Failure \boxtimes Fiber Breakage \blacksquare

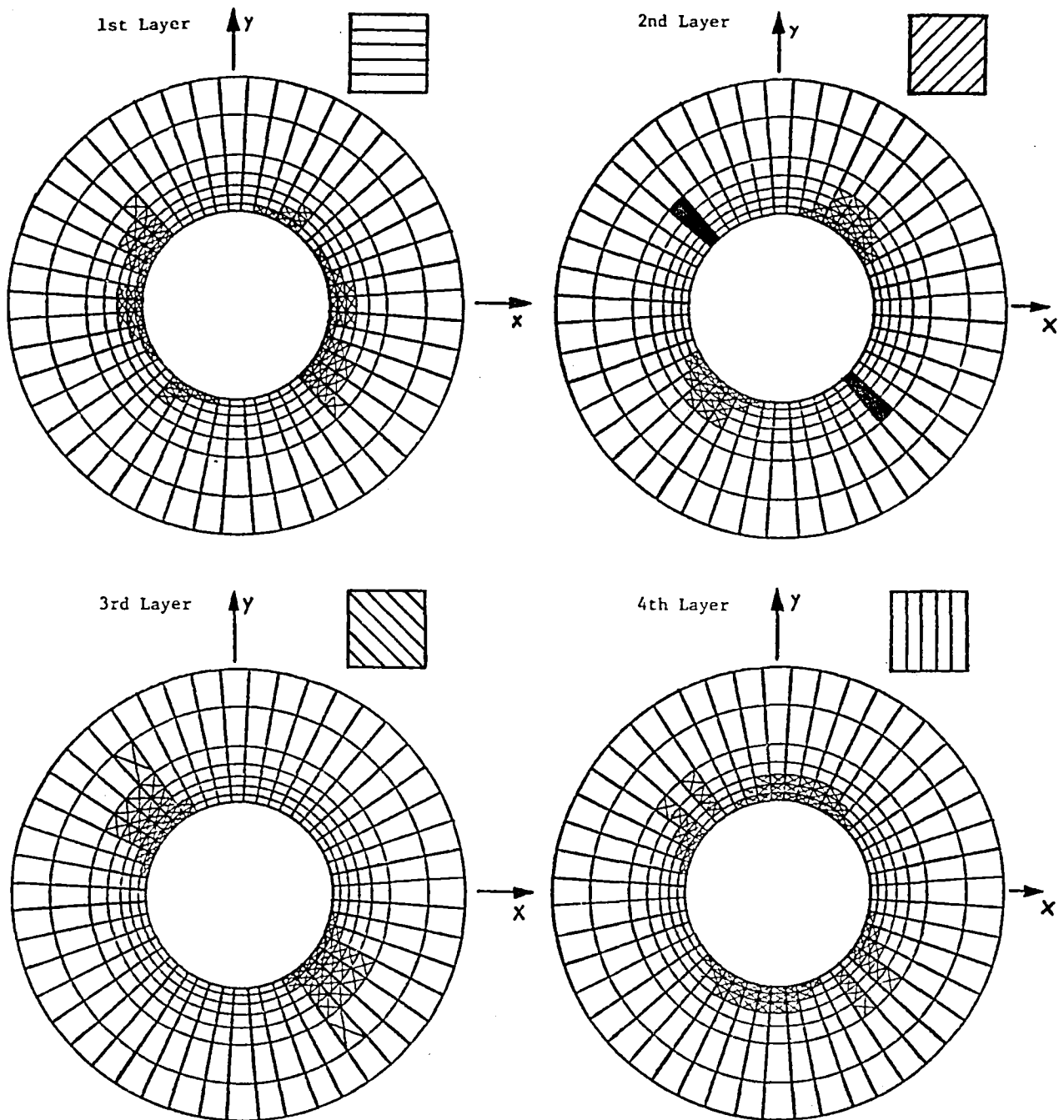


Fig. 25. Damage zone at $\sigma = 193$ MPa, $k = 0$. Matrix Failure \otimes Fiber Breakage \blacksquare

1
2
3
4
5

6
7
8
9
10

1. Report No. NASA CR-165793		2. Government Accession No.		3. Recipient's Catalog No.	
4. Title and Subtitle BIAXIAL TESTS OF FLAT GRAPHITE/EPOXY LAMINATES				5. Report Date October 1981	
				6. Performing Organization Code	
7. Author(s) Harold Liebowitz and Douglas L. Jones				8. Performing Organization Report No.	
9. Performing Organization Name and Address The George Washington University School of Engineering and Applied Science Washington, DC 20052				10. Work Unit No.	
				11. Contract or Grant No. NSG-1289	
12. Sponsoring Agency Name and Address National Aeronautics and Space Administration Washington, DC 20546				13. Type of Report and Period Covered Contractor Report	
				14. Sponsoring Agency Code	
15. Supplementary Notes Langley Technical Monitor: John D. Whitcomb Final Report - February 1, 1976 - December 31, 1980 Appendix by James D. Lee					
16. Abstract <p>The primary purpose of this research program was to examine, analytically and experimentally, the influence of biaxially applied loads on the strength of composite materials containing holes. The analysis was performed through the development of a three-dimensional, finite-element computer program that is capable of considering three types of damage: fiber breakage, delamination, and matrix failure. Realistic failure criteria were established for each of the failure modes, and the influence of biaxial loading on damage accumulation under monotonically increasing loading was examined in detail.</p> <p>The experimental portion of this program encompassed both static and fatigue testing of specially designed biaxial specimens containing central holes. Initially, static tests were performed to obtain an understanding of the influence of biaxial loads on the fracture strength of composite materials and to provide correlation with the analytical predictions. The predicted distributions and types of damage were in reasonable agreement with the experimental results. Then a number of fatigue tests were performed to determine the influence of cyclic biaxial loads on the fatigue life and residual strength of several composite laminates.</p>					
17. Key Words (Suggested by Author(s)) Composite materials Biaxial loading Finite-element analysis Fracture Fatigue			18. Distribution Statement Unclassified - Unlimited Subject Category 24		
19. Security Classif. (of this report) Unclassified	20. Security Classif. (of this page) Unclassified	21. No. of Pages 106	22. Price A06		

1
2
3
4
5

6
7
8
9
10

DO NOT REMOVE SLIP FROM MATERIAL

Delete your name from this slip when returning material to the library.

NAME	MS
Kunigal Shivakumar	188E